Department für Chemie

Exploiting avidity in chimeric antigen receptors (CARs) to increase safety and specificity of CAR T cell therapy

Master Thesis

zur Erlangung des akademischen Grades
"Diplom-Ingenieur" (Dipl.-Ing.)

eingereicht von
Michael Schöber, BSc. Wien, 1.11.2019

Betreuer: Univ. Prof. Mag.rer.nat. Dr.rer.nat. Christian Obinger
Mitbetreuer: Dr.rer.nat. Dr.habil.med. Manfred Lehner

Die Arbeit wurde in der St. Anna
Kinderkrebsforschung in Wien durchgeführt

Acknowledgement

Firstly, I want to thank Wolfgang Holter in whose group I received the chance to work and Christian Obinger who supervised this work gave valuable feedback.

Many thanks go to my wonderful PI Manfred Lehner. He was wonderful in guiding me through my work at the CCRI, both personally as well as professionally. From him I learned a lot about scientific writing and presentation skills, as well as how to properly structure ideas and make them understandable for others.

I want to express a lot of gratitude to Benjamin Salzer, who was my main supervisor during my time at the CCRI. Benjamin taught me a broad spectrum of new things, ranging from laboratory techniques to planning and structuring of experiments. In terms of how to organize myself and work precisely and properly I was able to learn a lot from Benjamin. He went out of his way to make sure I could work in a good environment and sacrificed a lot of his time for me.

Special thanks go also to my former colleague and good friend Christina Schüller, without whom I would not have come to the CCRI, as it was her who made me aware of the open position as a master student in this lab. During my first two months at the CCRI we worked together and I learned a lot from her. Her resilience, structure and excellence served as an example for myself to aspire to.

During Benjamins stay at the University of Oxford Charlotte Brey took care of me, especially by helping out with my experiments at BOKU. I want to thank her a lot for that.

Konstantin Byrgazov shared his wealth of knowledge about Osteosarcoma with Manfred and I, which was invaluable for our bioinformatics project. Apart from that I got to know him as an incredibly supportive person, who was always willing to exchange new ideas and have a good laugh over lunch.

The bioinformatics part of this work could not have grown to what it turned out to be now without the help of Niko Popitsch and Florian Halbritter from the CCRI, as well as the input of Peter Sykacek. Thank you!

I am very grateful to have shared time at the CCRI with my fellow master student Paula Hofbauer, who was always there during breaks, to share experiences and grab a coffee with. We had a lot of good times and I am glad to be able to call her a friend now.

Lastly, I want to thank my family and friends who always supported me when I was having difficult times personally during the time of my thesis. I want to especially acknowledge my mother Maria, my father Karl, my friends Magda, Matthias, Yu and Max and my sister Victoria. I feel very blessed for having you all in my life.

Table of contents

List of Figures

List of Tables

Abbreviations

CAR	Chimeric antigen receptor
IFN-γ	Interferon gamma
IL-2	Interleukin 2
hEGFRt	Truncated human epidermal growth factor receptor
hHER2t	Truncated human epidermal growth factor receptor 2
TAA	Tumor-associated antigen
OS	Osteosarcoma
ICOS	Inducible T-cell co-stimulator
Treg	Regulatory T cell
ELISA	Enzyme-linked immunosorbent assay
CTL	Cytotoxic T lymphocyte
Treg	Regulatory T cell
T_h	T helper cell
TCR	T cell receptor
MHC	Major histocompatibility complex
ITAM	Immunoreceptor tyrosine-based activation motif
Ig	Immunoglobulin
B-ALL	B cell acute lymphoblastic leukemia

Abstract

A lack of potency, as well as safety, are the two main hurdles to making chimeric antigen receptor (CAR) T cell therapy more applicable for a wider range of malignancies. For conventional CARs, targeting only one tumor associated antigen (TAA), these two aspects are however opposed to one another. One possible solution to this problem is the construction of AND-gate CARs, which require the presence of two or more target antigens to trigger a response. This could vastly reduce on-target/off-tumor toxicity and would thus allow for generation of much more potent CARs for the treatment of solid tumors.

In previous work, our group developed a novel CAR format in which avidity can be exploited to integrate AND-gate function into CARs. These novel types of CARs with AND-gate function are based on the defined heterodimerization of two different CAR molecules comprising a low-affinity binding domain specific for an antigen A *and* antigen B, respectively. Efficient T cell activation by these novel heterodimeric CARs depends - due to the low affinities of the individual binding domains - on bivalent interaction, i.e. avidity. Furthermore, the function of these avidity-dependent AND-gate CARs can be regulated by the addition of a small molecule that induces the heterodimerization of the two different CAR molecules. In a proof-of-principle study, an EGFR/HER2-specific AND-gate CAR was generated which enables specific killing of EGFR^{pos}/HER2^{pos} (double positive) target cells and is dependent on the presence of the small molecule AP21967.

The further improvement of this novel type of AND-gate CAR requires the screening of many different constructs. Thus, one of the goals of this work was to establish the functional testing of CARs in a reporter Jurkat cell line, as an option for "high-throughput" screening of CAR constructs. However, the cell line proved not to be generally suited for studies in the context of our AND-gate CARs. Therefore, the function of CAR constructs containing different co-stimulatory domains was tested in primary human T cells. Among the tested co-stimulatory domains (4-1BB, CD28, ICOS, CD2 and OX-40) the CD28 domain unexpectedly proved unsuitable for the generation of AND-Gate CARs. Furthermore, we developed and confirmed the functionality of a leucine zipper-based, constitutively active AND-gate CAR, which can be utilized for *in vivo* testing without the need for the frequent administration of a small molecule dimerizer. Lastly, we initiated a project to screen for potential tumor-specific antigen combinations in osteosarcoma (OS). We employed an *in silico* approach based on RNA sequencing (RNA-Seq) data of a variety of healthy tissues and compared this data to sequencing data from OS tissue samples from the INFORM registry. PANX3 and IFITM5, amongst others were identified as prime targets which could allow specific targeting of OS by CAR T cells.

Concluding, we were able to show that a CD28 co-stimulatory domain might adversely affect the efficacy of avidity driven AND-gate CARs and offered a proof of principle for a leucine zipper based constitutive AND-gate CAR. Lastly, on the basis of RNA-Seq data, we were able to single out potentially highly specific markers for safer targeting of OS by CAR T cells.

Kurzfassung

Mangelnde Wirksamkeit und Sicherheit gelten als die größten Hindernisse für eine breitere Anwendung der „chimeric antigen receptor"(CAR)-T-Zelltherapie. Im Falle von herkömmlichen CARs, welche nur auf einzelne Antigene abzielen, stehen diese beiden Aspekte jedoch im Gegensatz zueinander. Eine mögliche Lösung für dieses Problem ist der Bau von AND-Gate CARs, die das Vorhandensein von zwei oder mehr Zielantigenen erfordern, um eine Aktivierung der T-Zelle auszulösen. „On-target/off-tumor toxicities" könnten damit potentiell stark reduziert werden, was wiederum den Einsatz wesentlicher potenterer CARs, unter anderem für die Behandlung solider Tumore ermöglichen könnte.

Unsere Gruppe entwickelte dafür ein neuartiges CAR-Design, das eine AND-Gate Funktion über die Nutzung des Aviditätseffektes erreicht. Dieser CAR basiert auf der definierten Heterodimerisierung zweier separater CAR Ketten mit niedrig-affinen Bindungsdomänen, die jeweils Antigen A bzw. Antigen B erkennen. Die effiziente Aktivierung der T-Zellen hängt - aufgrund der geringen Affinitäten der einzelnen Bindungsdomänen - von der bivalenten Wechselwirkung, d.h. der Avidität ab. Darüber hinaus kann die Funktion dieser aviditätsabhängigen AND-Gate-CARs durch Zugabe eines „small molecules" gesteuert werden, welches die Heterodimerisierung der beiden verschiedenen CAR-Moleküle induziert. In einer „proof-of-principle"-Studie wurde ein EGFR/HER2-spezifischer AND-Gate-CAR generiert, der ermöglicht EGFR[pos]/HER2^{pos} Zielzellen gezielt anzugreifen und vom Vorhandensein des „small molecules" AP21967 abhängig ist.

Die weitere Verbesserung dieses neuartigen AND-Gate-CAR-Typs erfordert das Screening vieler verschiedener Konstrukte. So war eines der Ziele dieser Arbeit, die Funktionstests von CARs in einer Reporter Jurkat-Zelllinie zu etablieren. Die Zelllinie erwies sich jedoch als nicht geeignet für Studien im Rahmen unserer AND-Gate-CARs, weshalb die Funktion von CAR-Konstrukten mit verschiedenen co-stimulatorischen Domänen in primären menschlichen T-Zellen getestet wurde. Unter den getesteten co-stimulatorischen Domänen (4-1BB, CD28, ICOS, CD2 und OX-40) erwies sich die CD28 Domäne unerwarteterweise, aufgrund unspezifischer Aktivierung, als nicht tauglich für die Generierung von AND-Gate CARs. Weiters konnten wir einen Nachweis für die Funktionalität eines „leucine zipper"-basierten, konstitutiv aktiven AND-Gate CARs bringen. In der Folge könnte dieser CAR für *in vivo* Versuche, ohne die Gabe des „small molecules" AP21967, verwendet werden. Zuguterletzt sollten mögliche tumorspezifische Antigenkombinationen für das Osteosarkom identifiziert werden. Dazu wurden die Expressionsstärken aller Gene im Osteosarkom mit den jeweiligen Expressionsstärken in einer Reihe von gesunden Geweben mit der Hilfe von RNA-Sequenzierung verglichen. PANX3 und IFITM5 wurden unter anderem als attraktive Zielantigene identifiziert, die ein spezifisches Targeting von Osteosarkomzellen durch CAR-T-Zellen ermöglichen könnten.

Zusammenfassend konnten wir zeigen, dass eine CD28 co-stimulatorische Domäne die Wirksamkeit von aviditätsbasierten AND-Gate-CARs negativ beeinflussen könnte. Außerdem erbrachten wir einen „proof of principle" für einen konstitutiven AND-Gate-CAR, der auf „leucine zipper"-Domänen basiert ist. Schließlich konnten wir auf der Basis von RNA-Seq-Daten potenziell hochspezifische Marker für das Osteosarkom identifizieren, die für eine CAR-T-Zelltherapie genutzt werden könnten.

1. Introduction

In recent years, in addition to conventional means of cancer therapy such as radiotherapy, chemotherapy and surgery, a variety of methods and concepts – summarized under the umbrella term "immunotherapy" – have emerged, of which chimeric antigen receptor (CAR) T cell therapy is one of the most promising strategies.

CARs are proteins that combine the signalling capabilities of parts of the T cell receptor (TCR) complex with the specific antigen binding of antibody fragments or other binding scaffolds. The extracellular antigen binding domain is fused, via a transmembrane domain, to the intracellular signalling domains that are able to activate the T cell after target recognition. The signalling domains usually encompass the CD3ζ-domain, which directs and mediates cytotoxic T cell activity and cytokine release, and co-stimulatory domains derived from proteins such as CD28, 4-1BB and OX40, that intensify T cell activation, induce proliferation and enhance survival [1]. CAR T cells are very potent, hard to control living agents, which can potentially induce life-threatening side effects. Their application is therefore limited to a relatively small number of tumor-associated antigens (TAAs).

Most successes in the clinics were thus far achieved in treating refractory B cell malignancies targeting CD19. In 2017, Kymriah manufactured by Novartis and Yescarta by Kite Pharma were the first two CAR T cell therapies approved by the FDA. CD19, like all non-mutated antigens, is not tumor specific, this therapy leads to the depletion of healthy CD19 positive cells in the body, this being all cells of the B cell lineage. In contrast to many other tissues and cell types in the body, toxicities towards B cells are manageable, since patients with B cell aplasia can be treated with intravenous immunoglobulin (IVIG) replacement therapy [2]. In order to be able to expand CAR T cell therapy to other malignancies, especially also solid tumors, alternative approaches to target only one TAA at a time are needed.

1.1 How CAR T cells are generated

CAR T cells are genetically modified T cells that express an artificial CAR, usually consisting of an extracellular antigen binding domain in the form of an scFv, as well as the intracellular CD3ζ signalling domain of the naturally occurring TCR, in order to induce T cell activation. Later generations of CARs harbor additional co-stimulatory domains, such as CD28 or 4-1BB. Second generation CARs incorporate only one of these co-stimulatory domains, while third generation CARs include two or more. CAR T cell therapy involves harvesting of the patient's leukocytes, followed by enrichment for T cells via magnetic beads (see Figure 1). The enriched cell population is then activated and expanded with beads that mimic the stimulation by antigen presenting cells and transduced with the help of a viral vector. After quality control and formulation, the cell product is then frozen in order to be shipped to the infusion site. The manufacturing of the cells generally requires 5 – 10 days, while times from collection of the material until the administration of the product will generally range from 2-4 weeks In the meanwhile patients usually undergo a lymphodepletion regimen in order to enhance CAR T cell persistence as well as efficacy by reducing the activity of regulatory T cells (Tregs) [3], [4].
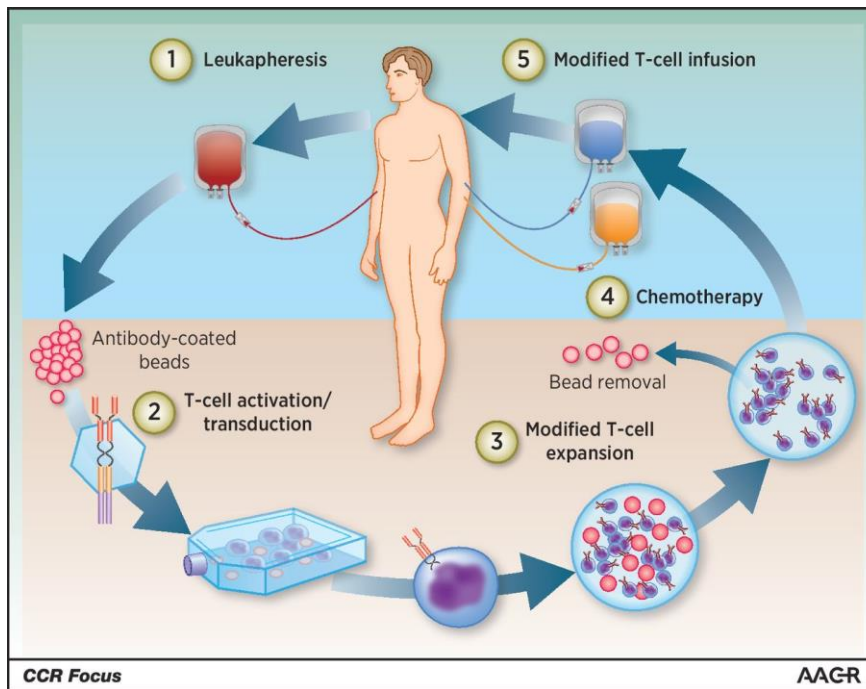
Figure 1: Production of CAR T cells
(M. V Maus and C. H. June, Clin. Cancer Res., vol. 22, no. 8, pp. 1875–1884, Apr. 2016)

1.2 Why use T cells to treat cancer?

Paul Ehrlich is generally credited as the first to suggest that the immune system protects against cancer in the year 1909. Ehrlich hypothesized that if it were not for the protective effects of the immune system, cancer would be very prevalent in large multi-cellular organisms. He is thus seen as the father of the theory of immune surveillance [5], [6].Whether this really was the case was disputed for a long time. After initially seeming likely, the hypothesis came into question in the 1970s when studies by Stutman et al. failed to generate convincing evidence by comparing the cancer susceptibilities of immunocompetent mice and mice with major immune dysfunction. Cancer rates turned out to be relatively similar in a large number of mice, thus the concept of immune surveillance was temporarily discarded [7], [8].

Starting from the 1990s however, different immunocompromised mouse models enabled the reconsideration of the immune surveillance hypothesis on the grounds of new and better evidence. For example Dighe et al. were able to show that mice lacking a functional Interferon gamma (IFN-γ) receptor were more vulnerable to spontaneous, as well as induced tumor formation[9], [10].

In 2001, it was discovered that the immune system not only acts as a tumor repressor, but also influences the tumors immunogenicity. This discovery changed the overall picture and was the stepping-stone from the concept of immune surveillance to the concept of cancer immunoediting [11].

Immunoediting is thought to take place in three stages: elimination, equilibrium and escape. During the elimination stage, transformed cells are detected by the immune system and disposed of. The formation of most tumors is halted during this phase. In some rare cases, however, tumor cells might initially escape detection and elimination by the immune system. They will then enter a phase of equilibrium, where cell death (induced by immune cells or otherwise) and cell growth in the tumor site are in balance. During this stage progressive selection for less immunogenic subclones in the tumor will take place. This can lead to tumor cell

variants that are no longer recognized by the immune system or are insensitive to immune cell mediated killing. When this becomes the case, the tumor may start to grow and cause symptoms in the patient [8], [5], [12].

Thus, already established tumors must have evolved mechanisms that not only allow them to circumvent limits on cell proliferation and avoid cell death, but also to allow them to escape immunosurveillance, all of which are now widely regarded as hallmarks of cancer [13].

CAR T cells can potentially bypass some of these resistance mechanisms, since CARs allow targeting of TAAs independently of presentation on the major histocompatibility complex (MHC). Additionally, CAR T cells can be "armored", meaning they express additional synthetic receptors or soluble factors, which allow them to resist the inhibitory tumor microenvironment [14], [15].

1.3 A short overview of the immune system and T cells

The immune system is generally divided into two parts; the innate as well as the adaptive immune system. The cornerstones of innate immunity are professional phagocytes (monocytes, macrophages as well as dendritic cells and natural killer cells) and the complement cascade (which also interacts with the adaptive immune system). T and B cells form the backbone of the adaptive immune system, which is defined by its main features of antigen specific recognition via T and B cells receptors as well as immunological memory, something that the innate immune system does not exhibit [16].

B cells carry the B cell receptor, a membrane bound variant of the immunoglobulins, or antibodies, which can bind an antigen specific to a particular B cell. Together with stimulation by T helper cells leads to full B cell activation. Five major classes of antibodies produced by B cells are known: IgM, IgG, IgA, IgE and IgD [17].

T cells on the other hand bear the signifying TCR on their surface, which is able to specifically recognize a vast variety of antigens and consequently activate the cell in the presence of said antigen. T cells can be subdivided into $CD8^{pos}$ cytotoxic T cells (CTL), $CD4^{pos}$ T-helper cells (T_h) and Tregs [18], [19].

1.3.1 CD8^{pos} T cells

CTLs are primarily defined by their expression of the CD8 co-receptor, which interacts with the MHC class I complex, which expressed by virtually all nucleated cells in the human body and is responsible for the display of endogenous peptides [20].

The main role of CTLs in the immune system is the constant monitoring of almost all nucleated cells in order to detect any abnormalities that could become a danger to the integrity of the organism. This includes both cells infected by viruses as well as malignant tumor cells [21].

CTLs can be classified into four distinct phenotypes according to their expression of CD45RO and CCR7: Naïve T cells ($CCR7^{pos}/CD45RO^{neg}$), central memory ($CCR7^{pos}/CD45RO^{pos}$), effector memory ($CCR7^{neg}/CD45RO^{pos}$) and terminally differentiated effector T cells ($CCR7^{neg}/CD45RO^{neg}$) [21], [22].

There are two different main mechanisms of cytotoxicity in CTLs. Firstly, the FAS pathway: CTLs carry the FAS-ligand, which interacts with the FAS receptor on the surface of the target cell. Triggering of the FAS receptor

induces trimerization of the receptor and thus engagement of the intracellular associated death domains. This leads to apoptosis of the affected cell via the classical pathway [18], [23].

Alternatively, CTLs can release perforin and granzyme into the cleft of the immunological synapse. Granzymes are able to enter the target cell through channels formed by the porins and initiate apoptosis through interaction with a variety of downstream targets (at least three distinct pathways), including caspase-3 and caspase-9. Additionally, Granzyme A is also able to induce cell death in a caspase-independent manner, through disruption of the mitochondria [24].

1.3.2 CD4^{pos} T cells

Four main types of CD4^{pos} T cells are known. These include Tregs cells as well as T$_h$1, T$_h$2 and T$_h$17 cells. The CD4 receptor expressed by these cell types, similarly to CD8, acts as a co-receptor to the TCR in the interaction with the MHC class II complex. MHC class II is usually found on the cell surface of professional antigen-presenting cells such as macrophages, monocytes, dendritic cells and B cells and is responsible for the presentation of extracellular proteins [19].

T$_h$1 differentiation is driven mainly by the cytokines IL-12 and IFN-γ. This type of helper T cell enhances mainly the cellular immune response towards intracellular parasites, while T$_h$2 cells mainly boost the humoral immune response and responses towards larger extracellular parasites such as helminths. IFN-γ secreted by T$_h$1 cells is responsible for the activation of phagocytes such as macrophages and microglial cells. T$_h$2 cells on the other hand secrete cytokines such as IL-4 and IL-13 [19].

T$_h$17 cells are a subtype of T helper cells characterized mainly by their production of interleukin-17 A and F, which are deemed to be pro-inflammatory. They mediate and enhance the immune response to primarily smaller extracellular parasites such as bacteria and fungi. T$_h$17 cells' differentiation is initiated by low levels of TGF-β in combination with IL-6, as opposed to Tregs, where high levels of TGF-β are critical to their lineage commitment [19].

Tregs are characterized by their expression of the biomarkers CD25 and FOXP3, the latter being a transcription factor also essential for Treg differentiation. Tregs can induce tolerance to a variety of antigens. They are therefore essential for the maintenance of the gut homeostasis, however, they also play a role in cancer progression. Tumor infiltration of CD4^{pos}/FOXP3^{pos} T cells correlates with a negative prognosis for most cancers, although the state of the evidence thus far remains controversial [25], [26].

The overall importance of CD4^{pos} T cells is illustrated quite dramatically by HIV, where without anti-retroviral treatment the infection will lead to a progressive loss of CD4^{pos} T cells. As a result patients suffer from systematic immune dysfunctions (acquired immune deficiency syndrome - AIDS), which can result in death [27].

1.3.3 TCR triggering

Activation of T cells is initiated via the TCR, which is unique for every individual T cell in a person's body. The TCR comprises an α and a β chain, which together form one peptide binding site. The activating signal is not transmitted by the TCR itself, but by the associated CD3 complex, consisting of εδ, ζζ, εγ-dimers [28], [29].

The α and β chains are composed of a variable extracellular domain involved in binding of peptides, a constant extracellular domain, a transmembrane region and a cytoplasmic tail. The diversity of variable T cell receptor regions is generated similarly to those of antibodies or B cell receptors: During T cell development in the thymus the TCR locus undergoes V(D)J recombination in every individual cell [30].

There are multiple competing, albeit not mutually exclusive, hypotheses regarding the molecular mechanism of TCR triggering. The oligomerization (or clustering) hypothesis postulates that activation of the TCR and phosphorylation of the associated ITAMs (Immunoreceptor tyrosine-based activation motif) happens through autophosphorylation of the receptors and associated Lck (lymphocyte-specific protein tyrosine kinase) once a sufficient local concentration of the receptor is reached. The second hypothesis proposes a conformational change. The pulling force applied to the TCR by binding of a peptide-MHC complex is thought to induce a conformational change, which exposes the ITAMs and enables their phosphorylation by Lck. Alternatively, it has been proposed that this conformational change enables clustering of multiple TCRs, thereby possibly enhancing kinase activity. So far, however, it is not entirely clear how exactly a pulling force would be transmitted to the interior of the cell and subsequently to the ITAMs [31], [32].

Another type of proposed mechanisms focuses on the fact that the TCR is embedded in the plasma membrane together with inhibitory molecules such as CD45. Indeed, it has been shown that Lck can be constitutively active independently of TCR engagement and that treatment of T cells with tyrosine kinase inhibitors leads to increased ITAM phosphorylation. Thus, the hypothesis suggests that TCR triggering might be a consequence of redistribution of the TCR away from inhibitory molecules. One possible mechanism is that as the cell membranes of T cell and target cell come into close contact with one another, through interaction of TCR and the peptide-MHC complex, CD45 and also CD148, which have large protruding ectodomains are being pushed away from the area of interaction. Without close proximity to the TCR, inhibition can no longer take place [31], [32].

Finally, the serial triggering hypothesis was popularized by Valitutti et al. in 1995 and seeks to reconcile the observation that already a very small number of specific peptide-MHC complexes (1-10) are sufficient to trigger a large number of TCRs and thus activate the T cell. It is not concerned with the exact molecular mechanisms of TCR triggering, however, it tries to explain the interplay of multiple receptors with each other. The interaction between the TCR and the loaded MHC complex tends to have low affinities and high off-rates. Valitutti et al. provide evidence that one loaded MHC complex could trigger more than 200 TCRs by specifically binding and then rapidly dissociating again from the receptor [28].

1.3.4 Downstream signalling

Downstream, the successful activation of the TCR leads to the phosphorylation of the ITAMs contained in the CD3 chains associated with the TCR. CD3 does not have an inherent autocatalytic activity, instead it is phosphorylated by the proteins Lck and Fyn, who belong to the Src family of protein tyrosine kinases (PTKs). Lck is recruited to the site by the CD4 or CD8 co-receptors, to which it is bound. CD4 and CD8 are in close proximity to the TCR complex through binding of the MHC (Figure 2). Fyn is also recruited to the site and together with Lck it is activated by CD45 through dephosphorylation of the C-terminal regulatory tyrosine residue. The Src PTKs then phosphorylate the ITAM motifs in the CD3 chains, which enables the recruitment of the kinase ZAP70 via its SH2 (Src Homology 2) domains. ZAP-70 is able to trigger a variety of downstream pathways, affecting functions such as cytokine production, and recruitment of the cytoskeleton, leading to formation of the immunological synapse, cell division and cell survival [31], [33].

More specifically ZAP-70, via intermediate steps, induces tyrosine phosphorylation in PLC-γ1, leading to the enzymes activation, which consequently catalyzes the production of the second messengers IP3 (inositol 1,4,5-triphosphate) and DAG (1,2-diacylglycerol) from the membrane lipid phosphatidyl inositol-4,5-bisphosphate (PIP2). IP3 is able to bind to calcium channels in the endoplasmic reticulum and trigger the release of Ca^{2+} ions. In the presence of an increased calcium concentration, the protein calmodulin activates the serine/threonine phosphatase calcineurin. Calcineurin then dephosphorylates the transcription factor NFAT, which can thus pass through the nuclear pore complex into the nucleus, where it binds to its partner AP-1 leading to the formation of nuclear NFAT (NFATn).

NFATn induces the transcription of genes related to T cell activation such as IL-2 and other effector molecules. Additionally, the production of DAG leads to triggering of protein kinase C theta (PKCθ), which activates factors CARMA-1, BCL-10 and MALT1. This finally invokes the important transcription factor NF-κB. Other pathways relevant in T cell activation include the TSC1/2-mTOR and the Ras-Erk1/2-AP1 pathway [31], [33].
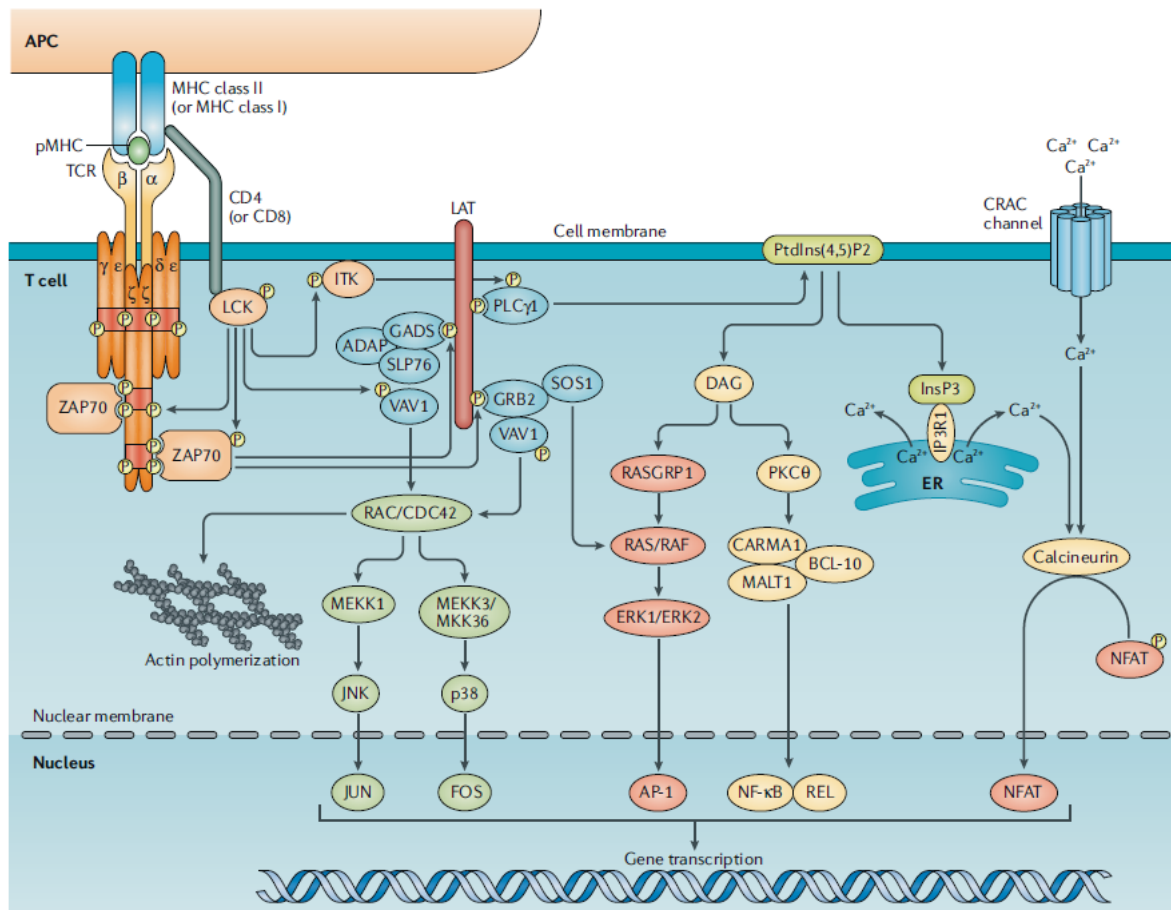
Figure 2: TCR signalling pathways: Engagement of the T cell receptor leads to ITAM phosphorylation, which triggers downstream signalling leading to the activation of a variety of pathways, such as the AP-1, NF-κB and NF-AT pathways
(G. Gaud, R. Lesourne, and P. E. Love, Nat. Rev. Immunol., vol. 18, no. 8, pp. 485–497, Aug. 2018 [34].)

1.3.5 T cell co-stimulation

In addition to positive binding events of the TCR, the full release of T cell effector functions additionally requires so called co-stimulatory signals, as well as cytokine stimulation, a concept termed the three signal hypothesis [35].

T cell activation without these additional signals will lead to T cell anergy, a state in which the T cells become activated but cannot proliferate [36]. Thus, for proliferation and full activation, T cells need a co-stimulatory signal (this is generally termed the classical two signal hypothesis). This signal can be provided by receptors such as CD28, 4-1BB, ICOS and OX40 (Figure 3). In the context of CAR T cells CD28 is thought to provide the strongest signalling response, however this has been shown to lead to early T cell exhaustion and potentially less antitumor activity *in vivo*. [37] 4-1BB in contrast has been shown to be able to partially rectify T cell exhaustion caused by tonic signalling of CARs [38].
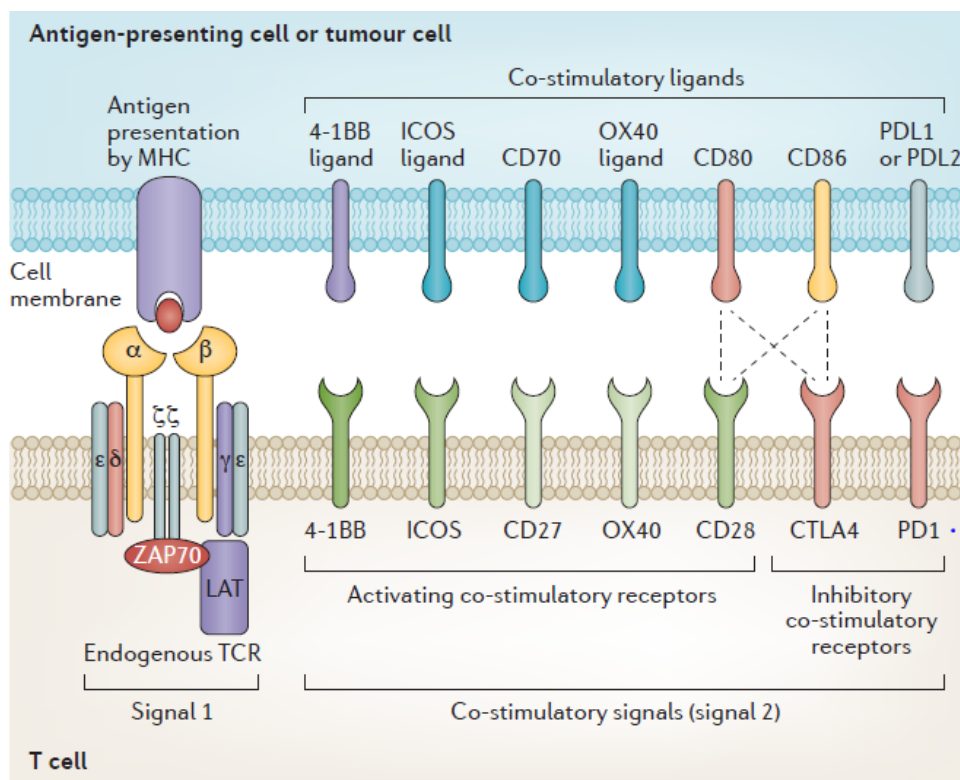
Figure 3: T cell co-stimulation
(A. D. Fesnak, C. H. June, and B. L. Levine, Nat. Rev. Cancer, vol. 16, no. 9, pp. 566–581, Sep. 2016. [4])

1.4 CARs

1.4.1 Architecture of CARs

The first ever devised CAR consisted of the variable regions of a monoclonal antibody fused to the constant regions of the α and β chains of a TCR [39].

First-generation CARs consisted of an scFv-binder fused to the CD3ζ domain via a hinge region and a transmembrane domain. Second generation CARs included a co-stimulatory domain in the form of CD28 or 4-1BB on top of that. Third generation CARs combine multiple co-stimulatory domains such as CD28 and 4-1BB to enhance signalling as well as CAR T cell persistence [4].

1.4.2 The current state of CAR T cells in the clinics

Thus far, two different CAR T cell products were approved by the FDA as therapeutics both directed against CD19, one for treatment of acute lymphoblastic leukemia (ALL) and one for relapsed or refractory diffuse large B-cell lymphoma. The approval of the former was based on the ELIANA trial, which showed complete remission rates of 82.5% for refractory B cell ALL [40].

Axicabtagene ciloleucel, the latter CAR product approved by the FDA, could demonstrate complete remission rates of 52%, while conventional treatments for this patient cohort resulted in mere 9% complete remissions.

In contrast to these studies, a variety of others have shown less promising results. Rates of complete remissions in the treatment of chronic lymphatic leukemia for example were merely 29%. In the treatment of solid tumors CAR T cells fare even worse: Two patients showed a response, while 5 displayed stable disease (out of 11 patients enrolled overall) in a study of EGFR-targeted CAR T cells for the treatment of non-small lung cancer. This trend extends to other trials of CAR T cells in solid tumors. Additionally CAR T cells for the treatment of solid tumors show severe toxicities in pre-clinical models, such as in the case of a disialoganglioside (GD2)-specific CAR for the treatment of neuroblastoma, where CAR T cells were administered to mice . After administration CAR T cells localized to the brain, consequently proliferating and causing severe tissue damage in the region, which ultimately proved to be lethal to the mice [41], [42].

1.4.3 Factors limiting the efficacy of CAR T cells

The reasons for lacking efficacy in many cancer types apart from B cell malignancies are manifold and reach from T cell exhaustion induced by tonic signalling of the CAR to a suppressive tumor microenvironment [43].

At this point it is relatively well established that tumor cells intrinsically create an environment that hampers the function of immune cells. A multitude of mechanisms are behind this phenomenon, presence of regulatory T cells, myeloid-derived suppressor cells, cancer-associated fibroblasts and tumor associated macrophages being some of them. The balance of polarization in tumor-associated macrophages might be skewed towards an M2-like phenotype, in part owed to constant apoptotic cell death occurring, which has been known to have immunosuppressive effects [44], [45], [41].

It has also been shown that the amino acid arginine plays an important role in shaping the tumor microenvironment. The semi-essential amino acid is known to be essential both for the function of immune cells as well as tumor cell growth and acts as a double edged sword in tumorigenesis [46], [47].

1.4.4 Important CAR associated toxicities and adverse events

Safety is one of the most important aspects being discussed today for CAR T cell therapy due to the large risks associated with the treatment. The main toxicities associated with CAR T cell treatment are on-target/off-tumor toxicities, cytokine release syndrome (CRS), neurotoxicities and anaphylaxis [48].

1.4.4.1 CRS

The most prevalent adverse effect linked to CAR T cell infusion is a pathological over-activation of the patient's immune system, caused by the overbearing release of cytokines. CRS has also been observed as a consequence of therapeutic monoclonal antibody or interleukin-2 administration. Elevations in cytokine levels include IFN-γ, GM-CSF, IL-10, and IL-6. Symptoms of CRS can include high fever, malaise, fatigue, myalgia, nausea, anorexia, tachycardia/hypotension, capillary leak, cardiac dysfunction, renal impairment, hepatic failure, and disseminated intravascular coagulation. Severe CRS can be potentially life-threatening. These symptoms are displayed in 18 – 43% of patients receiving a CD19 CAR product. The intensity of symptoms tends to correlate with the tumor burden as well as the degree of activation and proliferation of the administered CAR T cell product. Interestingly, it has been shown that the severity of the condition might ultimately be caused by the

release of IL-1, IL-6 and nitric oxide by host macrophages, as opposed to the by CAR T cells themselves [48], [49].

1.4.4.2 On-target/off-tumor toxicities

Since CARs do not usually target neoantigens, virtually all CAR targets exhibit overlaps in expression between cancerous and healthy tissues. The recognition of TAA[pos] healthy tissues by CAR T cells can lead to their destruction. This phenomenon is termed on-target off-tumor toxicity. Its severity can extend from cell lineage depletion, as in the case of the CD19 CAR with regards to B cells, to potentially life threatening conditions [42], [48].

1.4.4.3 Tumor cell transduction

A case report shows the potential dangers of the accidental retroviral transduction of leukemic tumor cells with the CAR construct. Ruella and co-authors describe the relapse of a patient nine months after administration of tisagenlecleucel (Kymirah). A single leukemic B cell had been accidentally transduced. The CD19 CAR that was consequently expressed on the surface of the cell and bound its ligand CD19 in cis position, thus effectively masking the epitope on the cell. This single clone was then able to undergo massive expansion, ultimately leading to the death of the patient [50].

1.4.5 Approaches for enhancing safety and specificity of CAR T cells

A variety of approaches have been developed to avoid and manage these adverse consequences which includes suicide switches, control through small molecules (ON-switches), adaptor-based CARs as well as NOT or AND-gate CARs.

1.4.5.1 Suicide Switches

Suicide switches work via the expression of artificial caspases that are inducible via administration of a small molecule and work as an emergency approach to treat acute strong cases of CRS or unforeseen target/off-tumor toxicities. An already approved elimination system is the iCasp9 system, which can be triggered by the small molecule dimerizer drug AP1903. The system was already successfully used in the clinics in order to treat graft-versus-host disease (GVHD) developed by four patients who had undergone stem cell transplantation followed by administration of genetically modified T cells for acute leukemia. A single dose of AP1903 was enough to eliminate the majority of the T cell product and end the GVHD [51], [52], [53].

1.4.5.2 ON-Switch CAR

ON-switch CARs are a class of CARs that allow for activation of an otherwise inactive receptor by a small molecule. This goes hand in hand with the possibility for fine tuning and gradual escalation of the CAR T cell's activity, simply by administering increasing doses of the small molecule. This has the natural advantage that the elimination of the T cell product is not necessary in order to regulate its potency [54].

An example of this was achieved by equipping T cells with a split CAR, one half of which carries a target antigen-specific scFv-fragment, the other half carrying intracellular signalling domains. The two independent

membrane bound proteins can interact via their heterodimerizable domains upon addition of a small molecule dimerizer, thus producing a functional CAR [55].

1.4.5.3 Adaptor based CARs (Universal CARs)

One more approach for controlling CAR T cell activity is based on using a CAR, consisting of two separate parts: A membrane bound part comprising the intracellular signalling domains, as well as an extracellular interaction domain (for example a leucine zipper) and a soluble, titratable adaptor fragment. This adaptor interacts with the membrane bound part of the CAR (possibly via a complementary leucine zipper) and also mediates the recognition of the TAA, for example via an scFv [54].

An example for such a CAR is the "SupraCAR" published by J. H. Cho et al. in 2018. The system combines a membrane-bound second-generation CAR fragment carrying an extracellular RR leucine zipper domain with a tumor targeting, soluble adaptor protein. The adaptor protein is constructed of a TAA-binding scFv domain and a leucine zipper EE domain, which interacts with the CAR. This allows for a variety of useful options. It enables fine tuning of CAR T cell activity though titration of the adaptor protein. OFF-switch behavior can be achieved, though competitive inhibition. The system also naturally allows for changing the targeted tumor antigen in the case of relapse or resistance, by simply switching the administered adaptor protein. Finally, by utilizing a first generation CAR and a separate chain with a co-stimulatory domain a simplistic version of combinatorial antigen input can be achieved [56].

1.4.5.4 Boolean logic gate CARs (NOT-gates and AND-gates)

CARs can be engineered to work as a Boolean logic gate more specifically NOT- or AND-gates. These approaches are mainly being implemented in order to mitigate the issue of on-target/off-tumor toxicities A NOT-gate saves a target cell from T cell mediated killing under the condition that it expresses a certain marker, which inactivates the T cell. Such CARs can be based on the naturally occurring PD-1 (Programmed cell death protein 1), which usually interacts with PDL-1 (Programmed cell death ligand 1) as its ligand. PD-1 is expressed on T cells and other immune cells and attenuates TCR mediated T cell activation and cell proliferation, by inhibiting the phosphorylation of ZAP70, a protein involved in the downstream signalling of the TCR.

In order to construct a NOT-gate an antigen specific binding domain is fused to the intracellular signalling domain of PD-1. This antigen has to be expressed on vital organs or cell populations, which would be at risk of elimination by the CAR T cells [51], [57].

AND-gates on the other hand integrate two input signals to one output signal, the input being the presence of two or more markers, the output being T cell activation and target cell killing. Importantly, the markers should be concomitantly expressed on a given cell for T cell activation. In 2016, Lim at al. first published a functioning AND-gate-CAR. The system consisted of a synthetic Notch receptor (synNotch), with an extracellular scFv-based antigen-binding domain recognizing GFP. Binding of the synNotch receptor drives the expression of a CAR directed against CD19. The authors showed that this system enables combinatorial antigen recognition both *in vitro* and *in vivo* (murine model). Potential safety issues still have to be considered with this system. Where two types of bystander cells, each expressing one of the antigens needed for CAR T cell activation, are co-localized, expression of the CAR might be triggered by the first cell type, leading to the subsequent destruction of the second cell type. Additionally the system utilizes the GAL4 promoter derived from yeast and is therefore always potentially immunogenic in humans [58].

Sukumaran et al. published a novel approach for enhancing potency and safety of CAR T cells. The approach is based on the expression of three individual synthetic receptors on the surface of the engineered T cells. Firstly, a first-generation CAR recognizing the prostate stem cell antigen (PSCA), secondly a receptor consisting of the extracellular domain of the transforming growth factor beta (TGF-β) receptor, fused to an intracellular 4-1BB co-stimulatory domain and finally to enhance activity and deliver cytokine stimulation to T cells, the authors used an inverted cytokine receptor (ICR) containing the IL4R (interleukin-4 receptor) ectodomain fused to the IL7R (interleukin-7 receptor) endodomain. Both TGF-β and IL-4 are generally regarded as "anti-inflammatory". Thus, an inhibitory microenvironment around the tumor, associated with high local concentrations of TGF-β as well as IL-4, is used to provide co-stimulation as well as cytokine stimulation to the CAR T cell. The paper demonstrated both *in vitro* as well as in murine models that all three signals are necessary for full activation, proliferation and survival of the T cells. T cells expressing solely the PSCA-specific CAR did display significant lysis of target cells *in vitro*, however, in the murine model only target cells expressing all three factors were eradicated [59].

It is of note that in a human this approach might be less specific due to the fact that human TGF-β and IL-4 will be endogenously expressed at many sites in the body. More generally, cytokines such as IL-2 also have a strong effect on T cell differentiation, which could replace the need for IL-4 as "signal 3" entirely. The mouse model probably underestimates some of these unspecific interactions, as it is likely that murine cytokines are in many cases not able to stimulate human cells to the same degree as autologous cytokines could [60], [61].

In terms of eliminating minimal residual disease (MRD) or micrometastases, targeting of soluble factors, present in the microenvironment of bigger lesions, might lead to issues as well, as below a certain tumor size soluble factors might not be concentrated enough to guarantee T cell stimulation. Overall this approach still shows great promise, as it allows targeting of three factors, some of which can be soluble factors as well [59].

1.5 DESeq2

DESeq2 is a package for R and a well-integrated tool for the analysis of RNA-Seq data. Mainly, it is used to calculate differential expression of genes between different biological or experimental conditions. It was published by Michael Love et al. in 2014 and is embedded in the larger bioconductor environment, a large array of interdependent methods and instruments for the analysis of high-throughput sequencing data. [1] One of DESeq2's advantages is that it enables testing of hypotheses from a very small sample size, which is often the case with RNA-Seq, due to limitation of sample material or merely for financial reasons. It does so by Empirical Bayes shrinkage, which allows the sharing of information between genes, based on the assumption that genes with similar expression strength have similar dispersion levels. This can be assumed in part because genes with very low read counts tend to have relative large variances (as seen in Figure 4) [62].

---

[1] https://www.bioconductor.org/
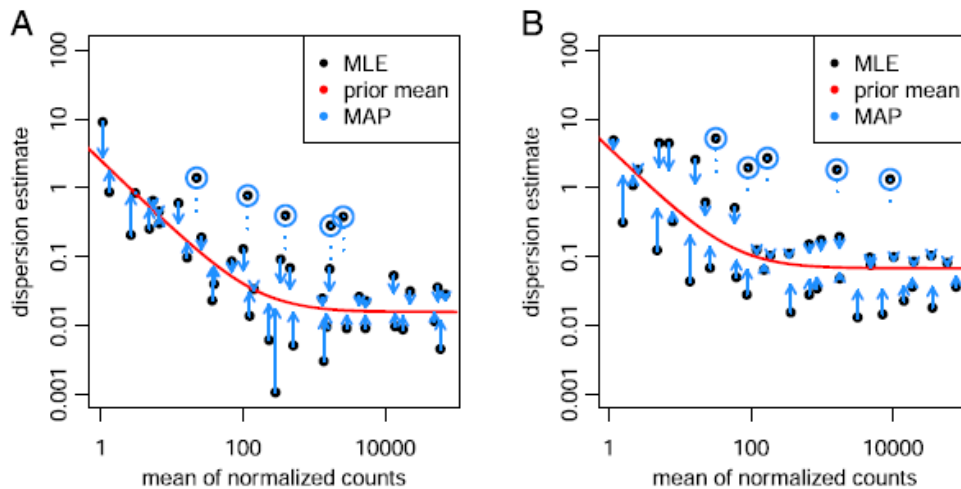
Figure 4: Principle of shrinkage estimation of dispersion with DESeq2: Initially, variance is calculated on a per gene basis (maximum likelihood estimation - MLE). Then estimation of the overall trend over all genes is fitted (prior mean) and variances are corrected towards this overall trend. The method also implements an outlier test. Strong outliers are assumed to have an underlying biological reason and are thus not adjusted (black dots in blue circles). A and B show two examples of this process. (M. I. Love, W. Huber, and S. Anders, Genome Biol., vol. 15, no. 12, pp. 1–21, 2014. [63])

1.6 Osteosarcoma

OS is a malignant neoplasm of the bone forming tissue. It is characterized by uncontrolled growth of spindle cells of mesenchymal origin and deposition of immature osteoid matrix. The peak incidence occurs in children and teenagers (OS accounts for 5% of all neoplastic malignancies in childhood), as well as above the age of 70 with the vast majority of cases originating in the long bones of the extremities (Figure 5). Current standard treatment involves neoadjuvant (reduction of tumor mass before surgical removal), chemotherapy with doxorubicin, cisplatin and in some cases Methotrexate. This regimen is followed by surgery, which involves either amputation of the affected limb, or a specialized limb salvage procedure [64], [65].
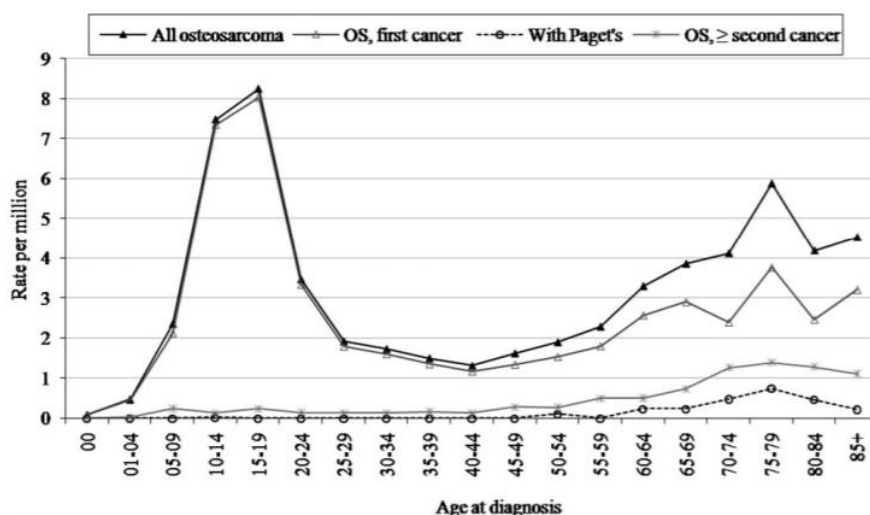
Figure 5: Bimodal age distribution of Osteosarcoma incidence.
(D. C. Allison et al., Sarcoma, vol. 2012, no. March. 2012. [66])

Prior to the introduction of chemotherapy OS used to be a universally fatal disease, with metastatic patients surviving only a few weeks. It was only during the 1980s with the broader introduction of chemotherapy into the treatment regimen for OS that survival rates saw a sharp increase from 11% to about 60% generalized across all stages of the disease (Figure 6). However, outcomes have remained relatively stagnant ever since. While for localized disease the prognosis is relatively good with a 5-year survival rate of 77%, metastasis to distant parts of the body leads to an average survival rate of merely 27% (combining patients with metastasis at diagnosis and relapse patients). For the former category, survival rates are even lower, with only 5-10% expected to survive for five years. It is for these reasons that better treatment options for patients with refractory, metastatic and recurrent disease are urgently needed [66].
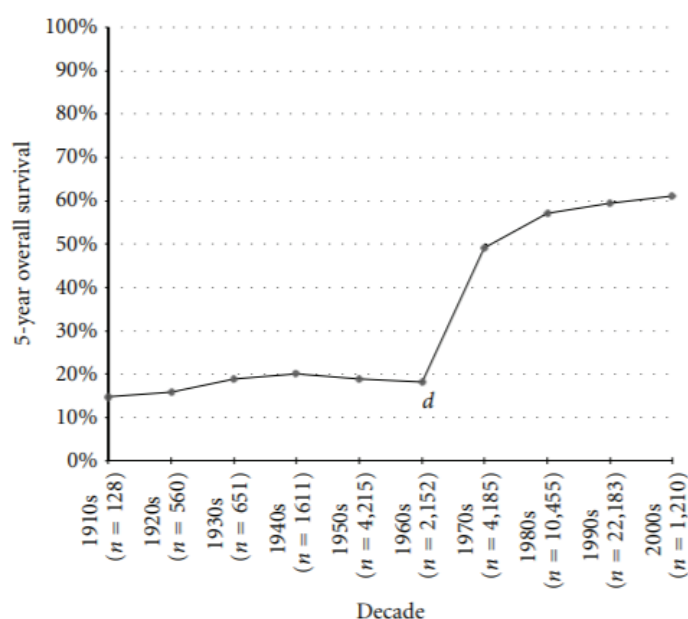
Figure 6: Development of 5-year overall survival rates in Osteosarcoma over the last century.
(D. C. Allison et al., Sarcoma, vol. 2012, no. March. 2012. [66])

A variety of new targeted therapies is in development, many of which try to harness tumor-specific dysregulation of cellular signalling on the one hand and the patient's immune system on the other hand to fight the disease. P53 is thought to be an important player in OS pathogenesis. A study by Overholtzer et al., 2003 found TP53 aberrations in 38% of the analyzed samples. Additionally, TP53 mutations were founds to be significant prognostic markers for survival of patients with OS [67], [68].

In OS development, also the mTOR pathway, downstream of IGF-1, is involved. This pathway is responsible for cell survival and proliferation, as well as angiogenesis. The drug Sirolian was found to inhibit metastasis and growth of OS in a xenograft model. CAR T cell therapy, after exhibiting rates of complete remissions in B-ALL of upwards of 80% is also under investigation for the purpose of treating OS. A variety of potential targets for this purpose have been investigated thus far including HER2, GD2, IL11-RA, fibroblast activation protein (FAP), IGF1R and ROR1 [64], [65].

A trial with a second-generation anti-HER2 CAR with a binding region based on the therapeutic antibody fragment FRP5, and a CD28 co-stimulatory domain was carried out by Ahmed et al in 2015 [69]. The study included 19 patients with HER2^{pos} tumors, 16 of which were OS, one Ewing sarcoma, one primitive neuroectodermal tumor and one desmoplastic small round cell tumor. The outcomes of the study were

modest, as only 4 out of the 17 evaluable patients enrolled in the study showed stable disease with durations between 12 weeks and 14 months. The median duration of survival for the 19 infused patients was 10.3 months. CARs targeting other markers are mainly still in the phase of *in vitro* testing or xenograft models [69],[70].

Targeting HER2 with CAR T cells has potentially life-threatening side effects. A publication by Morgan et al. (2010) describes the case of a women being treated for metastatic colon cancer that spread to liver and lungs, with HER2 specific CAR T cells, who died five days after the infusion of the CAR T cell product. The authors hypothesized that the administered cells had located to the lungs, where they came into contact with and recognized lung epithelial cells expressing low levels of HER2, leading to rapid respiratory failure, two cardiac arrests within 12 hours, gastrointestinal bleeding, the induction of a cytokine storm and finally death after 5 days in intensive care. This case highlights the importance of finding safer and more specific targets for CAR T cell therapy [71].

1.7 INFORM

The INFORM (INdividualized Therapy FOr Relapsed Malignancies in Childhood) consortium was built with the goal of establishing the infrastructure to enable personalized molecular therapies for relapsed/refractory disease in children and young adults (up until 21 years of age at the time of the detection of the primary tumor). Patients that receive tumor biopsy as a part of standard care for the following dignoses, are able to participate in the program: high risk-ALL,Post-stem cell transplantation-ALL acute myeloid leukemia, rhabdoid tumor, ependymoma, medulloblastoma, Ewing's-sarcoma, high-grade glioma (including diffuse intrinsic pontine glioma), high-risk neuroblastoma, non-Hodgkin lymphoma, OS, soft tissue sarcoma and rare tumor diseases in case of no established curative treatment. Next generation sequencing techniques are then applied to characterize the tumor and identify molecular targets for potential single case experimental treatments. Those targets are independently validated in a central pathology laboratory after a review process. The information is then deposited in a central registry in order to be used by the patient's treating oncologist in the hopes of improving the outcomes of patients (only about 10% of patients with relapsed disease can be cured at this moment).[2]

---

[2] https://www.dkfz.de/en/inform/

2. Aims

CAR T cell therapy, while being a very potent treatment option for patients with refractory B-cell malignancies, is associated with a variety of adverse conditions, some of which are potentially life threatening. This includes CRS, neurotoxicities and on-target/off-tumor toxicities. Therefore, this work focuses on the optimization of CARs with AND-gate and ON-switch function and the identification of potential tumor-specific antigen-combinations for the treatment of OS.

CARs are in most cases dimeric molecules, as their hinge and transmembrane regions are built partly from naturally dimeric proteins, for example CD8. Previously, Benjamin Salzer and Christina Schüller were able to show that monomeric CARs could be generated through the deletion of cysteines in the stalk regions derived from CD8α. Moreover, they created reduced affinity versions of binders directed against EGFR and HER2. Conditional dimerization of CAR molecules harboring these low-affinity binders allowed for bivalent interaction with the target antigens and thereby synergistic amplification of the individual affinities, i.e., the avidity effect. This enabled both ON-switch and AND-gate function, yet the CARs' efficacy was attenuated compared its wild type version. The goal of this work was to build on these prior findings and further optimize the system.

Firstly, a low-affinity hHER2 (human HER2)-specific binder, which had previously been functionally tested in the AND-gate CAR, should be further biochemically characterized. Hereto, the binder should be recombinantly produced and affinities subsequently determined by SPR. The second aim of this work was to optimize the efficacy of the avidity-dependent CARs by optimizing co-stimulation and testing the usability of Jurkat reporter cells for functional analysis in this context. Thirdly a constitutively active AND-gate CAR should be developed that does not depend on the administration of a heterodimerizer and thus facilitates *in vivo* testing. Finally, the fourth aim was to set up an *in silico*-screening method for identifying tumor-specific antigens or combinations thereof which could allow targeting of OS by CAR T cells.

3. Materials and methods

3.1 Materials

3.1.1 Disposables

Table 1: List of disposable items

Material	Manufacturer
Assay Plate 96-well round bottom white polystyrene	Costar
Cell culture flasks (25 cm², 75 cm², 175 cm²)	Thermo Fisher Scientific
Cryotubes	Thermo Fisher Scientific
Electroporation cuvettes 4 mm	VWR
ELISA Plates (96-well, maxisorp)	Thermo Fisher Scientific
Eppendorf® tubes 1.5 and 2 mL	Sigma-Aldrich Co. LLC.
FACS tubes 5 mL	BD Falcon™
Falcon tubes 15 mL, 50 mL	BD Falcon™
Microplate 96-well PP V-bottom	Greiner Bio-One GmbH
Pipette filter tips, sterile (10, 20, 200, 1000)	Thermo Fisher Scientific
Pipette tips (10-200 µL, 100-1000 µL)	Greiner Bio-One GmbH
Well plates (6-, 12-, 24-, 48-, 96-wells)	Thermo Fisher Scientific
Amicon Ultra-15 Centifugation Filter Unit	Merck

3.1.2 Miscellaneous products

Table 2: Miscellaneous products

Miscellaneous Products	Manufacturer	Ref. Nr.
Human CD3/28 T activator Dynabeads®	Thermo Fisher Scientific	11131D
AccuCheck counting beads	Invitrogen/Thermo Fisher Scientific	PCB100
B/B homodimerizer	Takara Clontech	635058
A/C heterodimerizer	Takara Clontech	635057
dNTP Mix 10 mM each	Biozym	331520
Recombinant Human IFN-γ (carrier-free)	BioLegend	570202
BD Quantibrite™ PE Phycoerythrin Fluorescence Quantitation Kit	Becton Dickinson	340495
Lumi-Film Chemiluminescent Detection Film	Sigma Aldrich	11666916001
Page-RulerTM Plus Prestained Protein Ladder	Thermo Fisher Scientific	26619
Mini-PROTEAN®TGXTM	Biorad	456-1083
IgG1, Kappa from murine myeloma clone MOPC21 (1 mg/mL)	Sigma Aldrich	M7894-5MG
Propidium iodide solution	Sigma Aldrich	P4864-10ML
Stericup® 0.45 µm, HV Durapore® Membrane	Millipore	SCHVU01RE
Recombinant Human IFN-γ (carrier-free)	BioLegend	570202
Subcloning Efficiency™ DH5α™ Competent Cells	Thermo Fisher Scientific	18265017
Bovine serum albumin (BSA)	Sigma Aldrich	A4503
Protein A chip	GE Healthcare	29127555
Fc-Her2	RD Systems	1129-ER-050

3.1.3 Cell culture

Table 3: Items used in cell culture

Cell Culture Products	Manufacturer	Ref. Nr.
0.05% Trypsin-EDTA	Gibco	25300-054
AIM V	Gibco	12055-083
Dimethyl Sulfoxide (DMSO)	Sigma Aldrich	D2650-100ML
Dulbecco's Phosphate Buffered Saline (DPBS)	Gibco	14190-094
Dulbeccos Modified Eagle Medium (DMEM)	Gibco	41965-039
Fetal Bovine Serum (FBS)	Sigma Aldrich	Lot: 035M3358
Hepes Buffer	Gibco	15630-049
L-glutamin 200 mM	Gibco	25030-024
octaplasLG	Octapharma	Lot: M649C9521
Opti-MEM	Gibco	11058-083
Penicillin Streptomycin (P/S)	Gibco	15140-122
RPMI 1640 W/GlutaMax –I	Gibco	61870-010
RPMI 1640 without phenol red	Gibco	11835-063

3.1.4 Composite media and buffers

Table 4: List of self-made buffers and media

Medium	Composition
10x TBE buffer	1 M Tris
	1 M Boric Acid
	0.02 M EDTA (disodium salt)
Ponceau S	purchased from Sigma Aldrich (Ref. Nr. P3504)
10x SDS running buffer	144 g/L glycine
	30 g/L Tris
	10g/L SDS
10x Western transfer buffer	140 g/L glycine
	30 g/L Tris
10x Western transfer buffer	10% (v/v) 10x Western transfer buffer
	20% (v/v) methanol
10x TBS	121 g/L tris
	175.2 g/L NaCl
	pH 7.5
TBST	10% (v/v) 10x TBS
	0.1% (v/v) Tween-20
Western Blocking buffer	10% 10x (v/v) Roche Blocking Reagent in TBS
PBS 10x	80 g/L NaCl
	2.03 g/L KCl
	27.19 g/L $Na_2HPO_4 * 7H_2O$
	2.40 g/L KH_2PO_4 monobasic
Equilibration Buffer	1.9 g/L NaH_2PO_4
	9.25 g/L $Na_2HPO_4 * 7H_2O$
	17.5 g/L NaCl
	Titrate to pH 8.0
1M Imidazole Elution Buffer	1.86 g/L NaH_2PO_4
	9.24 g $Na_2HPO_4 * 7H_2O$
	35 g NaCl
	68 g Imidazole
	Titrate to pH 8.0
Regeneration Buffer	3.94 g/L 2-(N-Morpholino)ethanesulfonic acid
	17.43 g NaCl
	to 1000 mL ddH20
	pH 5.0

Sonication Buffer	17.55 g NaCl
	1.857 g NaH$_2$PO$_4$ (119.98 g/mol)
	9.26 g Na$_2$HPO$_4$ * 7H$_2$O (268.07 g/mol)
	37.8 g Glycerol (1.26 g/mL)
	10 mL Triton X-100
	Titrate to pH 8.0
Lysogeny Broth (LB) Medium	10 g/L tryptone
	10 g/L NaCl
	5 g/L yeast extract
	(20 g/L agar)
	required antibiotics were added as 1000x stock
	ampicillin: 100 µg/mL final
	kanamycin: 50 µg/mL final
AIMV++++ culture medium	AIM V
	2.5% Hepes
	2% Octaplas
	1% L-glutamin
	200 U/mL IL-2
Cryoconservation medium	RPMI 1640 W/GlutaMax-I
	20% FBS
	10% DMSO
DMEM culture medium	DMEM, 10% FBS, 1% P/S
	10% FBS
	1% P/S
RPMI culture medium	RPMI 1640 W/GlutaMax-I
	10% FBS
	1% P/S
RPMI T cell medium	RPMI 1640 W/GlutaMax-I
	10% FBS
	1% P/S
	200 U/mL IL-2

3.1.5 Antibodies

Table 5: Antibodies for flow cytometry

Antibody	Manufacturer	Clone	Dilution
PE Ganglioside GD2 Antibody	BioLegend	14G2a	1:25
PE CD274 (B7-H1, PD-L1) Antibody	BioLegend	29E.2A3	1:25
PE CD243 (MDR-1) Antibody	BioLegend	UIC2	1:25
PE CD29 Antibody	BioLegend	TS2/16	1:25
PE CD13 Antibody	BioLegend	WM15	1:25
CD3 PE-Cy7	Becton Dickinson	SK7	1:50
CD4 PerCP	BioLegend	RM4-5	1:22
CD56 APC	eBioscience	MEM188	1:25
CD8 FITC	BioLegend	SK1	1:50
EGFR APC	BioLegend	AY13	1:50
EGFR PE	BioLegend	AY13	1:50
FLAG PE	BioLegend	L5	1:167
HER-2 PE	BioLegend	24D2	1:50
StrepII Biotin	GeneScript	5A9F9	1:500
StrepII PE	GeneScript conjugated with R-PE Conjugation Kit (Abcam, ab102918)	5A9F9	1:167

3.1.6 Enzymes

Table 6: Enzymes

Enzyme	Manufacturer	Ref. Nr.
2x Gibson Assembly Mastermix	New England Biolabs	M5510AA
2x HIFI DNA Assembly Mastermix	New England Biolabs	M5520A
DpnI	New England Biolabs	R0176S
Halt™ Protease Inhibitor Cocktail	Thermo Fisher Scientific	87786
Phusion Hot Start II High-Fidelity DNA Polymerase	Thermo Fisher Scientific	F549L
Pierce Universal Nuclease For Cell Lysis	Thermo Fisher Scientific	88700
Q5 Hot Start High Fidelity Polymerase	New England Biolabs	M0493L

3.1.7 Kits

Table 7: Kits

Purpose	Kit	Manufacturer	Ref. Nr.
Gel Extraction	QIAquick Gel Extraction Kit	Qiagen	28704
IFN-γ ELISA	Human IFN-γ ELISA Ready-Set-Go!	Thermo Fisher Scientific	88-7316
gDNA isolation	QIAmp DNA Blood Mini Kit	Qiagen	51104
In vitro transcription	mMESSAGE mMACHINE T7 Ultra Kit	Ambion	AMB1345-5
Medium scale plasmid DNA preparation	QIAfilter Plasmid Midi Kit	Qiagen	12243
Mycoplasma testing	MycoAlert PLUS	Lonza	LT27-288, -285, -291
PCR Purification	QIAquick PCR Purification Kit	Qiagen	28104
Protein quantification	Pierce BCA Protein Assay Kit	Thermo Fisher Scientific	23227
RNA purification	Rneasy Mini Kit	Qiagen	74104
Small scale plasmid DNA preparation	EasyPrep Pro Plasmid Miniprep Kit	Biozym	390052

3.1.8 Laboratory equipment

Table 8: Laboratory equipment and devices

Device	Manufacturer
Laminar Flow Hood NordicSafe®	Esco Micro Pte. Ltd.
Centrifuge Megafuge 1.0R	Heraeus/Thermo Fisher Scientific
Centrifuge Multifuge 3sr	Thermo Fisher Scientific Inc.
Centrifuge 5424	Eppendorf AG
Centrifuge 5415D	Eppendorf AG
Flow Cytometer BD LSRFortessa™	BD Biosciences

ENSPIRE Multimode Plate Reader	PerkinElmer
ÄKTA™ start	GE Healthcare Life Sciences
Frac30	GE Healthcare Life Sciences
Western Blot Developer Type 942/206	AGFA Healthcare N.V.
Thermocycler BIOER	Gene Touch
Heating Block Thermostat C	Eppendorf AG
Incubator Heracell™240i	Thermo Fisher Scientific
Microscope Axiovert 135	Carl Zeiss GmbH
Electroporator Gene Pulser Xcell™	Biorad Laboratories
Surface Plasmon Resonance Spectrometer Biacore T200 machine.	GE Healthcare Life Sciences
Plate Reader	ENSPIRE® Multimode Plate Reader, PerkinElmer VICTOR™ Multilabel Plate Reader, PerkinElmer

3.2 Methods

3.2.1 Cell culture

3.2.1.1 Cultivation of primary T cells

T cells were isolated from buffy coats delivered by the Austrian Red Cross, Vienna. Cells were suspended in cryo-conservation medium (see Table 4) and stored at -196°C in liquid nitrogen, after a minimum of 24 hours at -80°C to allow for gentler freezing. Aliquots with approximately 5 million cells were thawed and resuspended in RPMI + 10% FCS + 1% P/S with $2*10^2$ Units IL-2/mL. Additionally, Thermo Fisher Dynabeads Human T-Activator CD3/CD28 beads were added at a ratio of 1:1 to the cell suspension for T cell stimulation (25 µL bead suspension per $1*10^6$ T cells). Cell concentrations were determined three times per week according to the cell count protocol in order to keep cultures between 0.4 and $2*10^6$ cells/mL. At least half of the culture medium was exchanged every two days. Cells were used for cytotoxicity experiments between 10 and 20 days after activation with the Human T-Activator CD3/CD28 beads.

3.2.1.2 Cultivation of cell lines

Cell Lines (Jurkats and Nalm-6) were cultured in RPMI with 10% FCS as well as 1% P/S at 37°C with 5% CO_2. Cells were counted three times per week in order to keep the cell concentration between 0.2 and $1.5*10^6$/mL. Regular testing for mycoplasma contamination was carried out with the MycoAlert PLUS kit.

3.2.1.3 mRNA Electroporation

For electroporation, cells were washed with 20 mL serum- and phenol-free RPMI medium followed by 20 mL Opti-MEM in a 25 mL Sterilin tube. After completion of the washing steps, cells were carefully resuspended in an appropriate volume of Opti-MEM. 100 µL of cell suspension (with a maximum cell concentration of 10 x 10^6 cells/100 µL) were then transferred into a 4 mm cuvette together with the desired mRNA. The electroporation was carried out at 500 V for 3 ms (Jurkats) or for 5ms (primary T cells) with a square wave protocol and one pulse. Finally, cells were transferred into pre-warmed culture medium at a final concentration of approximately $1*10^6$ cells/mL.

3.2.2 Molecular biological methods

3.2.2.1 PCR

PCR was carried out according to the following protocol: An initial denaturation step at 98°C was held for approximately 40 seconds. Annealing was carried out at 50-72°C for 10-30 seconds according to primer melting point [3]. Extension was carried out at 72°C for 20 seconds per kilobase. Final extension was held at 2 minutes at 72°C and the PCR-product was cooled down to 4°C.

---

[3] https://tmcalculator.neb.com/#!/main

Table 9: PCR reaction

Component	25 µl Reaction	50 µl Reaction	Final Concentration
5X Q5 Reaction Buffer	5 µl	10 µl	1X
10 mM dNTPs	0.5 µl	1 µl	200 µM
10 µM Forward Primer	0.125 µl	0.25 µl	0.5 µM
10 µM Reverse Primer	0.125 µl	0.25 µl	0.5 µM
Template DNA	variable	variable	< 1,000 ng
Q5 Hot Start High-Fidelity DNA Polymerase	0.25 µl	0.5 µl	0.02 U/µl
5X Q5 High GC Enhancer (optional)	(5 µl)	(10 µl)	(1X)
Nuclease-Free Water	to 25 µl	to 50 µl	

3.2.2.2 Construction of CAR constructs

Constructs were assembled by Gibson Assembly according to the standard instructions of the manufacturer (NEBuilder® HiFi DNA Assembly Cloning Kit). While the exact architecture of the constructs varied, open reading frames of all constructs included a CD33 signal peptide for translocation to the plasma membrane, a binder scaffold (Sso7d or affibody based) directed against a particular target antigen, followed by two G4S linkers, affinity tags and CD8α backbone that stretches through the membrane. Intracellularly, the CD8α backbone was fused to a co-stimulatory domain, followed by a dimerization domain and finally CD3ζ. Specifically for *in vitro* transcription, a T7 promoter, as well as a Kozak sequence were added at the 5' end.

3.2.2.3 *In vitro* transcription

In vitro transcription (IVT) with the mMESSAGE mMACHINE™ T7 Transcription Kit was carried out according to the manufacturer's protocol. Efficacy of the tailing reaction was evaluated by agarose gel electrophoresis. After completion of the reaction, mRNA was purified with the RNeasy Mini Kit with an adapted protocol:

375 µL of RLT buffer supplemented with 3.75 µL of β−mercaptoethanol were mixed with 275 µL of absolute ethanol. IVT-reaction was mixed with 650 µL of buffer and applied to a column. The column was centrifuged and the flow-through was discarded. Subsequently, three washing steps were performed, firstly with 700 µL of RW1 and thereafter twice with RPE buffer. After drying, mRNA was eluted with 30 µL of sterile, nuclease-free water and stored at − 80°C.

3.2.3 Flow cytometry

3.2.3.1 Cell counting

Cell counting was performed by flow cytometry utilizing AccuCheck Counting Beads. 100 µL of FACS-buffer were mixed with 2 µL propidium iodide (1 mg/mL) for live/dead cells discrimination, 10 µL of counting bead suspension as well as 10 µL of homogeneous cell suspension.

Cells/mL $*10^6 = \dfrac{number\ of\ viable\ cells}{number\ of\ aquired\ beads}$ * correction factor*

3.2.3.2 Antibody stainings

Reactions were carried out on ice with pre-cooled buffer to avoid endocytosis. Approximately 10^5 cells were transferred to a clean flow cytometry tube. Washing steps were carried out by adding 1 mL of FACS-buffer and spinning down the cells at 515 g for 7 minutes in a pre-cooled centrifuge (4°C). After the first washing step, the buffer was removed completely by aspiration. 50 µL of blocking solution (10% normal human serum in FACS buffer) were added, followed by incubation for 10 minutes at 4°C. The desired amount of antibody was added directly to the blocking solution and the mix was incubated for a minimum of 25 minutes at 4°C in the dark. After two washing steps, the stained cell suspension was acquired on the flow cytometer. In the case of secondary antibodies being applied, the process was repeated again starting from the incubation with said antibody.

3.2.3.3 Chemically Induced Dimerization

FKBP dmrA, dmrB and dmrC domains were used for dimerization. AP20187 (B/B homodimerizer) was applied at a concentration of 10 nM, AP21967 (A/C heterodimerizer) at 500 nM. After the application of either dimerizer, cells were incubated for 30 minutes at 37°C in standard culture medium.

3.2.3.4 FACS based cytotoxicity assays

Two days prior to the assay, cultures of the primary T cells as well as targets cells were adjusted to a cell concentration of approximately $0.4*10^6$ cells/mL to restart exponential growth. In the afternoon of the next day, cells were electroporated according to the standard electroporation protocol described previously (3.2.1.3 mRNA Electroporation). On the day of the experiment cells were spun down at 500 g for 5 minutes and resuspended in an approximately 5-fold smaller amount of culture medium. Cell concentrations were determined by FACS and adjusted to the desired level ($0.8*10^6$ cells/mL for primary T cells and $0.2*10^6$ cells/mL for Jurkat target cells) with standard culture medium. Takara A/C (AP21967), B/B (AP20187) dimerizer were then added as needed to the cell suspensions followed by incubation for 30 minutes at 37°C. GFP^{pos}/target antigen^{pos} Jurkat cells were mixed at a 1:1 ratio with mCherry^{pos}/target antigen^{neg} Jurkat cells. 40,000 effector T cells were applied per well of a 96-well round bottom plate together with 20,000 cells of the target cell mixture (10,000 cells each). After mixing effector and target cells, the 96-well plate was spun gently at 300 g for 5 minutes in order to bring the cells into contact with each other before incubating the plate at 37°C. After 4 hours of incubation, cells were spun down at 515 g for 7 minutes in order to harvest supernatants for IFN-γ ELISA. Specific lysis was evaluated by flow cytometry, according to the following formula:

$$specific\ lysis = \left(1 - \frac{\dfrac{\%\ GFP+}{\%\ mCherry+}}{\dfrac{\%\ GFP+\ (target\ cells\ only)}{\%\ mCherry+\ (target\ cells\ only)}}\right)$$

3.2.3.5 Reporter Cell Line assay

Preparation of cells for the reporter cell line assay were done analogously to the FACS-based cytotoxicity assay with regards to effector cells. Target cells were regular Jurkat cells expressing the desired antigen (or no antigen).In order to distinguish reporter cells from target cells, reporter cells were transiently transfected with mRNA encoding dKeima or mAmetrine (both 1 µg mRNA), which have no spectral overlap with either GFP or CFP. This is important as target cells would otherwise be falsely counted as reporter cells. The respective dimerizer was added to cell suspensions as needed, followed by incubation for 30 minutes at standard

conditions. Reporter cells were then seeded at 20,000 cells per well and target cells at 10,000 cells per well in 50 µL each in a 96-well round bottom plate. Incubation times varied according to the particular experiment.

3.2.4 Production and purification of recombinant protein

3.2.4.1 Transformation and protein production

Chemically competent cells (Tuner D3 *E.coli)* were used as host cells. Affibody-based binder scaffolds were expressed with an N-terminal polyHIS-tag and a C-terminal sfGFP-tag in a pE-SUMO vector (Life Sensors). Minipreps containing the previously harvested plasmid were diluted with water (1:4) and 2 µL of the mix were added to the thawed competent cells. Incubation on ice for 30 minutes was followed by heat shock at 42°C for 30 seconds, 2 minutes incubation on ice and then regeneration in 950 µL SOC medium at 37°C for 40 minutes on the shaker. 100 µL of each suspension were plated on LB agar plates containing kanamycin and incubated overnight at 37°C. The following day, one clone for each binder (sfGFP-Her2-WT, R10A and R32A) was picked to inoculate 10 mL of LB medium with kanamycin. A glycerol stock was prepared the following day and stored at -80°C. Glycerol stocks were picked into 10 mL LB- medium supplemented with kanamycin and cultures were incubated overnight at 37°C. 500 mL of LB medium were inoculated with approximately 9 mL of stationary culture and incubated until an OD of 2 was reached. The cultures were then induced through addition of IPTG (Isopropyl β-D-1-thiogalactopyranoside) for a final concentration of 1 mM and incubated at 20°C overnight.

The cells were harvested by centrifugation at 5,000 g for 4°C for 20 minutes, the supernatant was discarded and the cells were resuspended in sonication buffer. Sonication was carried out at with the following settings: duty = 50%, intensity =5, duration = 2x 60 seconds (2 minutes cool-down period between single runs). Afterwards, the suspension was spun down at 20,000 g for 30 minutes at 4°C and the supernatant filtered (Steriflip – Millipore).

3.2.4.2 Purification

Protein purification was carried out using TAKARA TALON® Metal Affinity Resin, which binds to polyhistidine-tagged proteins. 3 mL of resin in ethanol were applied to a column and washed with 20 mL ddH$_2$O, followed by 20 mL of equilibration buffer. Imidazole was added to the protein supernatants to a final concentration of 10 mM. The protein supernatant was applied to and run through the columns twice, followed by washing steps with equilibration buffer containing 5 mM imidazole, then buffer containing 15 mM imidazole. The protein was then eluted from the column with 2x 7.5 mL equilibration buffer (250 mM Imidazole). Following the His-tag purification step, a buffer-exchange step with an Amicon Ultra-15 Centifugation Filter Unit (10 kDa Cutoff) was carried out. The total dilution of the buffer amounted to approximately 1:1,000. The final sample volume was 1.5 mL. Following the first purification step, the protein solution filter was again purified by preparative size exclusion chromatography (SEC) with an ÄKTA pure protein purification system. Fractions containing protein were pooled and then stored at -80°C. PBS supplemented with 200 mM NaCl was used as a running buffer and the system was operated at a flow rate of 1 mL/min. A HiLoad Superdex 200 column was used.

3.3 Surface plasmon resonance

SPR analysis of the binder variants was performed in the Biomolecular & Cellular Analysis (BmCA) Core facility at the University of Natural Resources and Life Sciences Vienna on a Biacore T200 machine. A protein-A chip

was used and pre-coated with HER2-Fc fusion protein. The sample was then applied to the chip in increasing concentration steps and the association of the zHER2-sfGFP binder fusion protein was measured.

The capture solution contained 4 µg/mL HER2-Fc and was applied to the chip for 60 seconds at a flow rate of 10 mL/min. For the WT binder variant, the contact time was set to 60 seconds and the dissociation time at the end of an individual run to 180 seconds. For the R32A and the R10A variants a contact time of 15 seconds and a dissociation time of 60 seconds were used. The flow rate was adjusted to 30 µl/min. Between individual runs, the chip was regenerated with a glycine HCl solution (pH=1.5), with a contact time of 30 seconds and a flow rate of 30 µl/min. We used a kinetics approach to quantify binding affinities, where the K_D value of a binder was calculated as the ratio of the individual k_{on} and k_{off} constants, which themselves were estimated by fitting the sensogram to a 1:1 Langmuir model using the Biacore T200 Evaluation Software (GE Healthcare).

3.4 ELISA

Experiments were carried out according to the standard protocol of BioLegend Human IFN-γ ELISA, except for sample and standard dilutions, which were done with cell culture medium (RPMI+ 10% FCS + 1% P/S). Recombinant human IFN-γ from BioLegend was used as standard.

3.5 Bioinformatic methods

3.5.1 Datasets

40 RNA-Seq datasets from OS-patients were obtained from the INFORM registry. Publicly available healthy tissue RNA-Seq datasets were downloaded from the Human Protein Atlas (https://www.proteinatlas.org/). Additionally, FASTQ files from a dataset entailing human mesenchymal stem cells as well as osteoblasts were obtained from the publishing groups via direct request. Our group was kindly assisted by Niko Popitsch, who downloaded most of the FASTQ files for all the healthy tissues from the Human Protein Atlas and mapped most of reads for both the OS data as well as the healthy tissue data with kallisto [72],[73].

We included samples from the following tissues and cell types: OS, adrenal gland, appendix, bone marrow, brain, colon, duodenum, endometrium, esophagus, fallopian tube, adipose tissue, gallbladder, heart, kidney, liver, lung, lymph node, mesenchymal stem cells, osteoblasts, ovary, pancreas, placenta, prostate, rectum, salivary gland, skeletal muscle, skin, small intestine, smooth muscle, spleen, stomach, testis, thyroid, gland, tonsils as well as urinary bladder.

3.5.2 Calculation of differential expression with DESeq2

Raw count tables provided by kallisto, comprising 216,741 different transcripts, were imported into R with the tximport package, thereby mapping them to gene level and summing transcripts belonging to the same gene. Differential gene expression was calculated between the OS cohort and all of the healthy tissue cohorts individually utilizing the package DESeq2 for R. DESeq2 internally normalizes for library size between samples and then utilizes a Wald test for hypothesis testing (see Figure 7 for a flowchart of data processing). To address the problem of multiple testing, DESeq2 uses a filtering approach based on the average expression strength of the gene across tissues in order to preselect candidates that are likely to be detected as differentially

expressed. The *P* values for genes passing the filtering are then adjusted for multiple testing with the Benjamini-Hochberg procedure [74]. The resulting outputs were saved as .txt files.

3.5.3 Obtaining tumor-specific markers

Genes counted as sufficiently differentially expressed for CAR targeting, with corrected value *P* values <= 0.05, as well as a log2 fold change ratios of greater than a specified cut-off (mostly a value of 6.5 was used here, meaning approximately 90-fold overexpression). Based on these conditions, each gene, for a respective comparison of OS versus any healthy tissue, was assigned a TRUE or FALSE value. Single genes differentially expressed when compared to all healthy tissues were selected. Alternatively, we also employed a ranking approach: Here, for every OS vs. healthy tissue comparison, we ranked all genes by their log2 fold change values. Out of the 34 tissue ranks per gene the lowest (worst) rank was then taken and all genes were once again ranked by their lowest tissue rank.
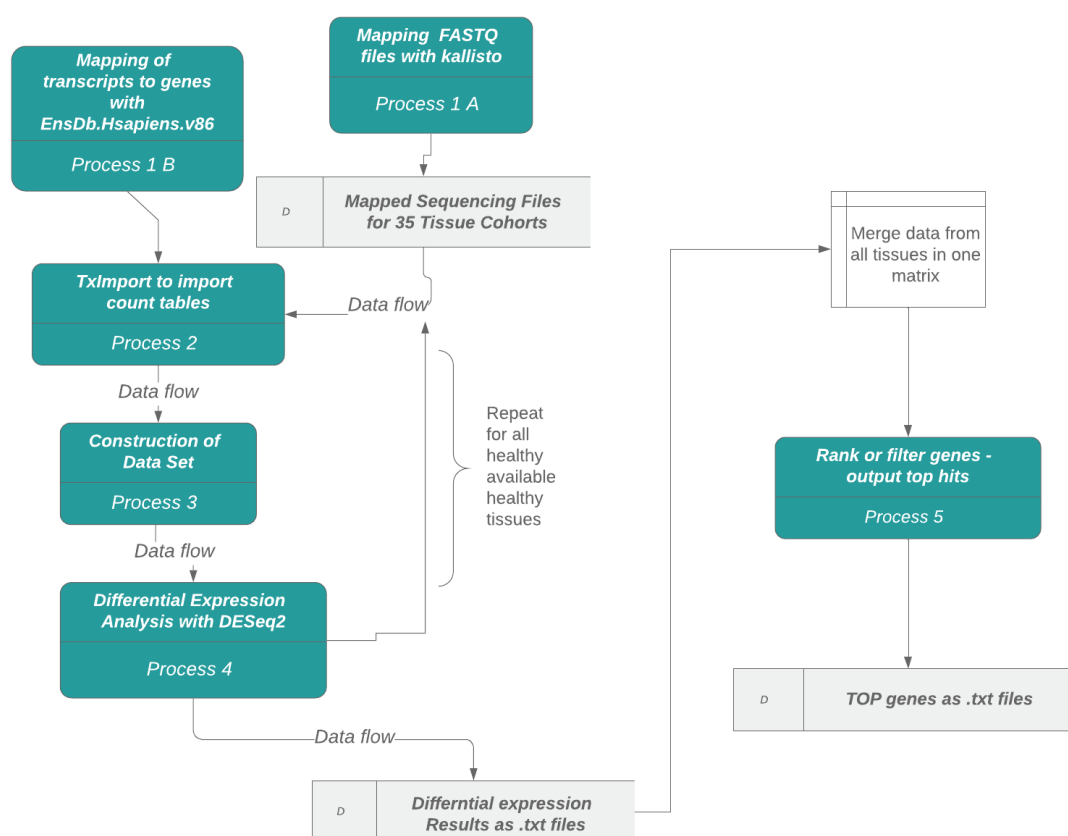
Figure 7: Overview of the pipeline used for RNA-Seq data analysis and subsequent screening for tumor-specific markers. Raw sequencing files were initially mapped with kallisto. For every comparison of OS vs. a healthy tissue all OS files and the respective healthy tissue files were imported to construct a DESeq2 data set.Differential expressions were calculated and the output was saved in a .txt file. This process was repeated for every healthy tissue, as to in the end receive 34 result files.These results were then merged in one large datatable, starting from which screening for OS specific single genes or pairs was carried out.

For gene pairs TRUE and FALSE values were evaluated based on an AND-OR logic. Diades of genes, where at least one gene out of two for every healthy tissue was differentially expressed, counted as a hit (see Figure 8). Additionally, we filtered for localization of proteins based on data available on the human protein atlas.

Comprehensive lists of proteins localizing to certain structures in the cell were downloaded from The Human Protein Atlas by selecting "Fields"-> "Subcellular Location" in the search bar and then entering the desired cellular location. See supplementary Table 2 for details on all tissue samples in our database.
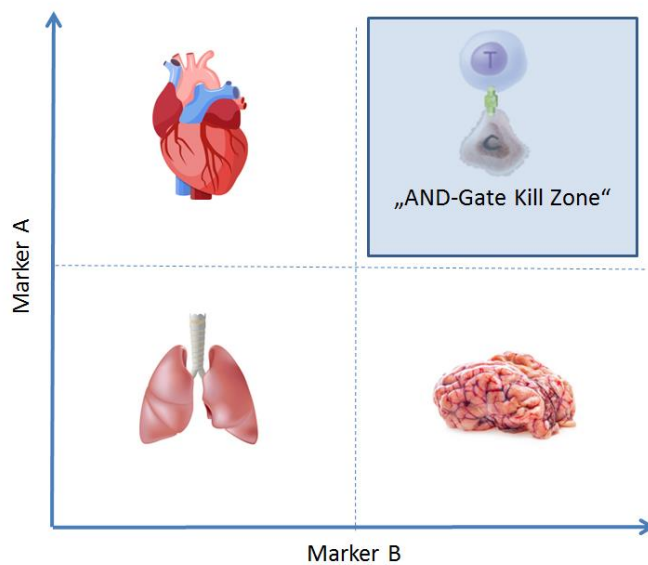
Figure 8: Illustration of an AND-gate in the context of CAR T cell therapy. In this simplistic model, the AND-gate consists of markers A and B. In the lungs expression levels of both markers A and B are either very low or zero. The brain exhibits high expression of marker B, while marker A is highly expressed in heart tissue. Tumor cells in this example, however, highly express both markers, facilitating their recognition by T cells, while bystander cells are spared.

4. Results

4.1 Functional screening for low affinity binder variants

The affibody zHer2.4 was modified by Benjamin Salzer in order to remove glycosylation sites. It was assumed that this would not substantially change the binder affinity since none of the mutated residues were involved in ligand binding. Affibodies are small binder molecules with a mass of about 6 kD, originating from the Z domain of *Staphylococcus aureus* protein A. 13 amino acids are involved in ligand binding of which the 12 non-alanine amino acids were mutated with the goal of identifying mutants that are suited for generating an avidity-based CAR. For this purpose, the binder mutants were integrated into CAR constructs which could be conditionally homodimerized by the small molecule AP20187 (B/B dimerizer). This strategy allowed for identifying the mutants which required bivalent interaction with the antigens for efficient T cell activation by the expressed CAR.
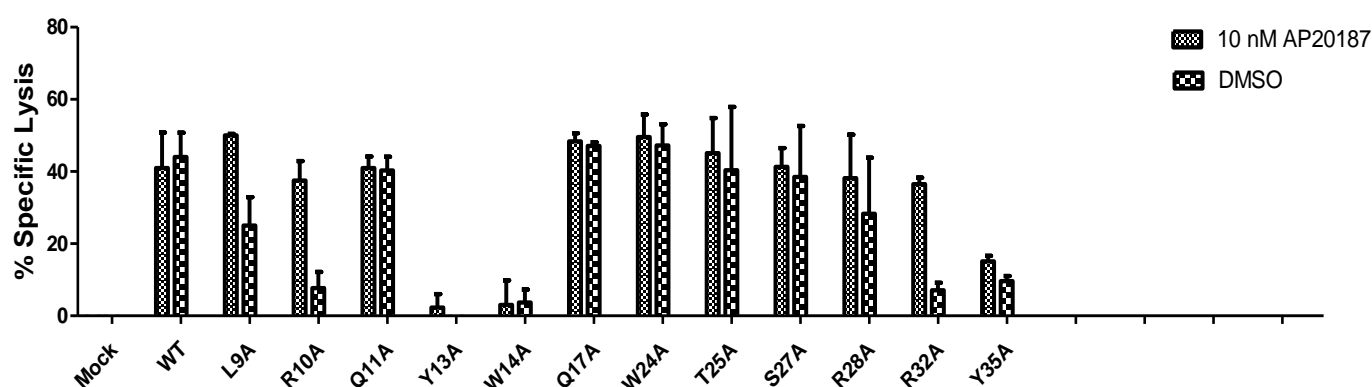

Figure 9: Functional screening of zHer2-AK affibody mutant versions: Figure shows the average of two independent experiments. Error bars indicate standard deviation. T cells were transiently transfected by mRNA-electroporation (5 μg) with the indicated CAR and Flow cytometry-based cytotoxicity assays were carried out. Target cells were hHER2t positive Jurkat cells (5 μg of mRNA) and mock Jurkat cells at a 1:1 ratio. The Figure shows the specific Lysis after 4 hours of co-cultivation, with or without the addition of small molecule dimerizer. Binder variants R10A, as well as R32A, result in high dependence of T cell activation on the B/B dimerizer.

In the dimeric state, i.e. in the presence of the B/B dimerizer, the CAR molecules containing the binder mutants R10A and R32A efficiently mediated lysis, which was comparable to the CAR containing the wild type binder, whereas lysis was low in the absence of the B/B dimerizer (see Figure 9). Thus, these two binders showed strong dependence on bivalent interaction and R10A was chosen for further characterization, as well as for integration in an affinity based AND-gate.

4.2 Binder production and SEC

The three hHER2-specific affibodies zHER2-AK and the mutants R10A and R32A were produced as fusion proteins with a C-terminal polyHIS-tag and a superfolder GFP (sfGFP) attached to the N-Terminus. The SEC profile of the binders showed an initial small shoulder followed by a steep peak (see Figure 10). Since this shoulder most likely indicates binder multimers, which could potentially interfere with later measurements, early fractions were discarded and only the fractions between the orange and green bars indicated in Figure 10 were pooled and concentrated. The product was then stored at -80°C in order to be used for further analysis.
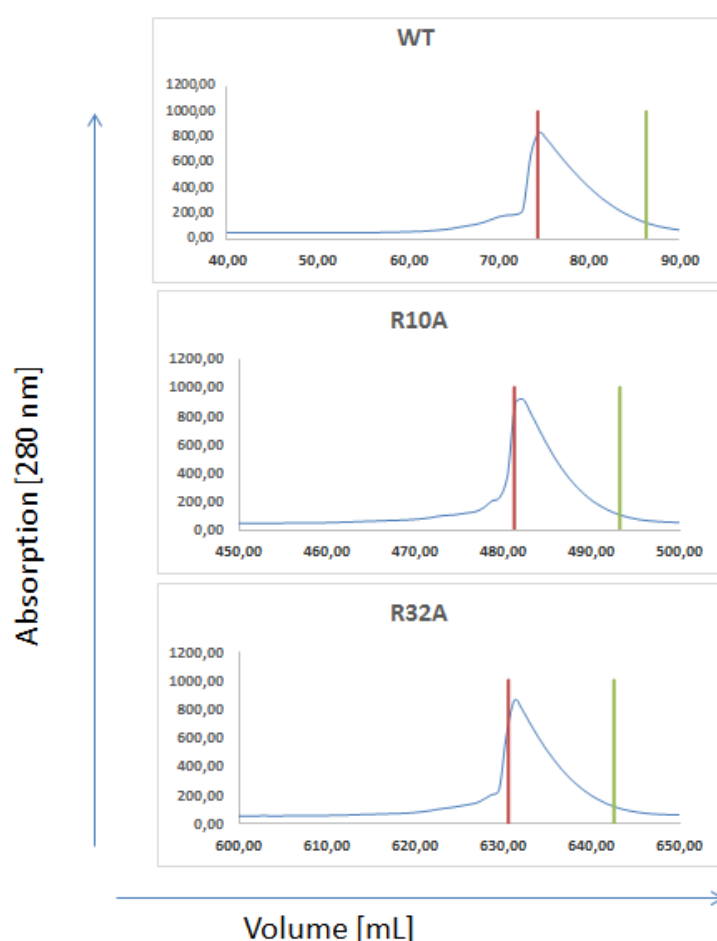
Figure 10: SEC profiles of WT zHER2.4 binder as well as mutant variants R10A and R32A: Affibody based binders were recombinantly produced in E.coli and subsequently purified by metal affinity chromatography followed by SEC. Parts of the curves between the red and green lines indicate fractions containing the purified monomeric binders.

4.3 k_{on} and k_{off} rates measured by SPR- switchable character of HER2 specific binders depends on binder affinity

k_{on} and k_{off} rates were determined for each binder variant by SPR with measurement parameters as described in the Methods section. Each binder variant was measured twice on two flow cells each and results were averaged (n = 4). Figure 11 shows representative measurement curves for each binder variant. The sample dilutions were carried out in a way that the assumed binder affinities would lie in the middle range of the dilutions. For the wild type (WT) binder, concentrations between 10 and 160 nM were chosen, for the binder variants R10A and R32A concentrations between 100 and 1600 nM, respectively, were used. The K_D-value of the wild type binder was determined to be 23 nM. Versions R10A and R32A had K_D values of 285 and 639 nM, respectively.
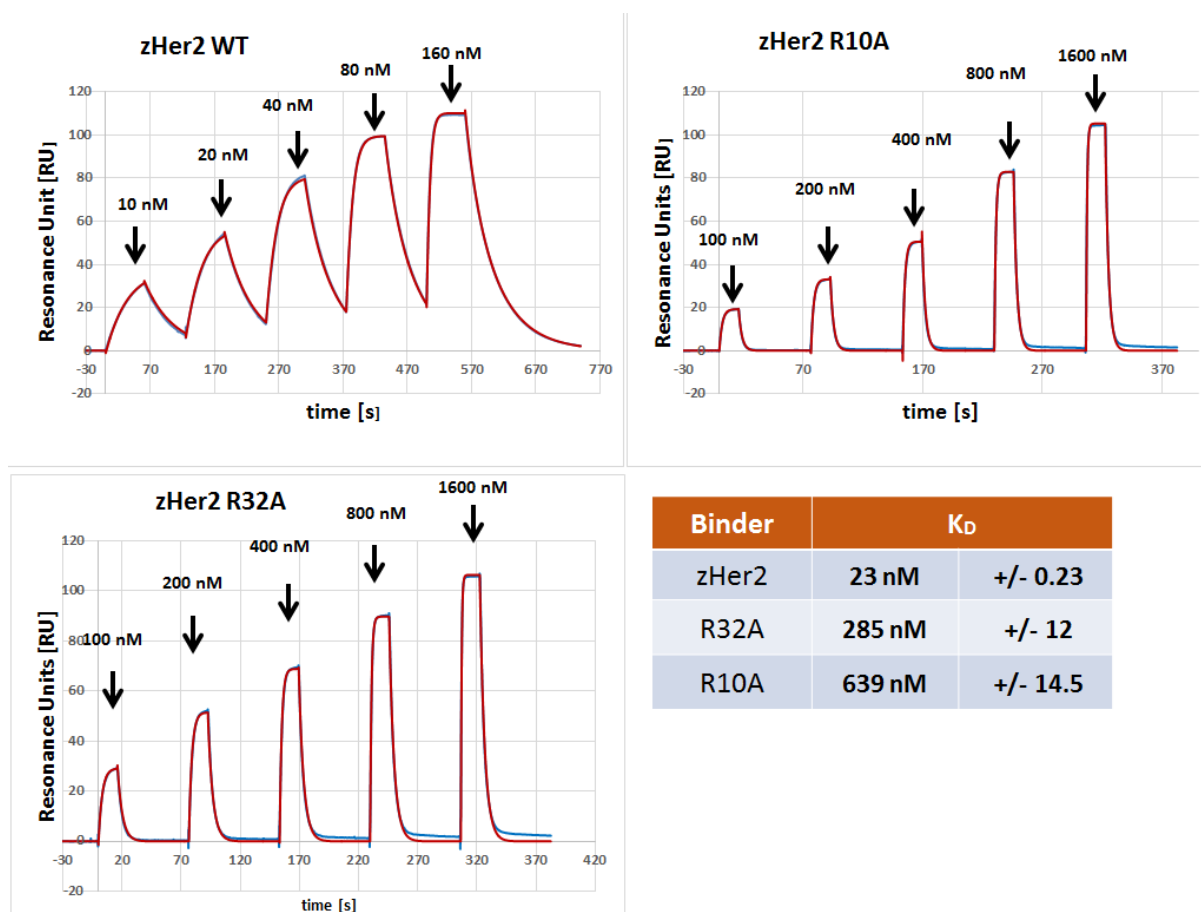
Figure 11: Determination of the affinities of the parental high-affinity zHER2-AK affibody, as well as previously selected mutant variants R10A and R32A. A protein A sensor chip was coated with recombinant HER2-Fc. The affibody variants were then titrated onto the chip in increasing concentrations in a single cycle mode, as detailed in the graph. Shown are representative curves from a total of four independent experiments; two per flow cell. Curves were fitted with a 1:1 binding model and kinetics-based determination of affinities was carried out.

4.4 Testing the suitability of Jurkat reporter T cells for evaluation of CAR function

The cell line used in the following experiments was a dual reporter Jurkat cell line (kindly provided by Peter Steinberger from the Medical University of Vienna) with response-elements for NF-KB and NF-AT driving the expression of fluorescence proteins GFP and CFP, respectively (see Figure 12 for graphical representation).
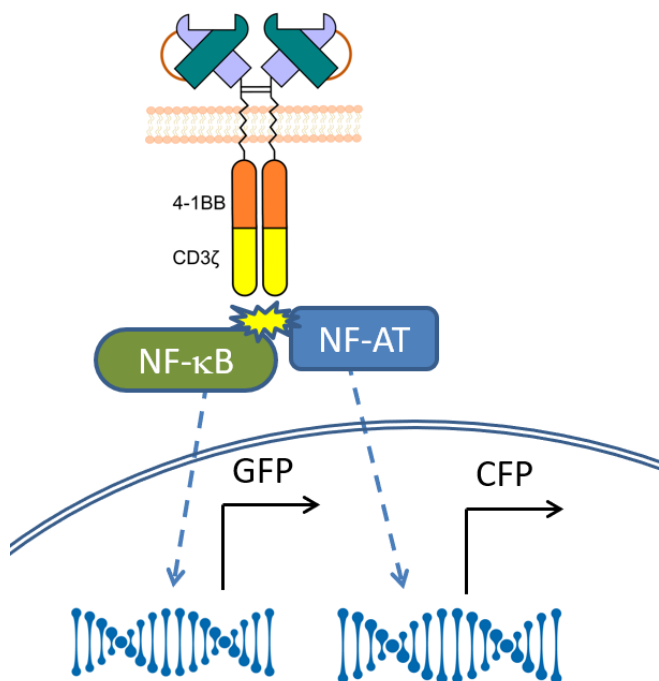
Figure 12 Graphical representation of the principle of the dual reporter Jurkat cell line: Engagement of the CAR triggers downstream signalling, leading to NF-kB and NF-AT localizing to the cell nucleus, where they drive the expression of reporter proteins GFP and CFP.

We generated CARs harboring 4-1BB, OX40, ICOS, and CD28 co-stimulatory domains. The constructs were tested in the dual reporter Jurkat cell line to verify the cell lines potential as a screening platform, since a cell line would offer some important benefits over primary T cells as a testing platform. Besides reduced cost and more flexible handling, Jurkat cell lines generally offer significantly higher protein expression levels than primary T cells. Therefore, constructs which are expressed in primary T cells only at low levels could still be evaluated when expressed in Jurkat cells. Figure 13a shows the general architecture of the CARs which consists of, going from extracellular N-terminus to C-terminus, a reduced affinity anti-human EGFR (α−EGFR)-specific Sso7d binder followed by two G4S linkers and an extracellular Strep II tag. A CD8α transmembrane region is followed by the respective co-stimulatory domain, an FKBP dimerization domain and a CD3ζ domain. Figure 13c shows scatterplots for the 4-1BB and OX40 CARs. For both CARs, NF-AT and NF-κB signalling was dependent on the presence of hEGFRt^{pos} (truncated human EGFR-positive) target cells, however, the CARs harboring a 4-1BB, ICOS, or CD28 co-stimulatory domain unexpectedly triggered a response even without the addition of AP20187, thus in what can be assumed is a monomeric state of the receptor. Only the OX40 CAR mediates dimerizer-dependent specific lysis. This stands in contrast to previous experiments of our group where it was shown that CARs harboring a 4-1BB co-stimulatory domain could efficiently trigger a signal in primary human T cells only after dimerization of the CAR by addition of AP20187. The overall stronger activation of the Jurkat cells observed with the 4-1BB CAR correlated with a higher expression of this CAR construct (Figure 13b).

Together, the fact that dependence of the function of the 4-1BB CAR on dimerization by AP21087 was clearly lost in the Jurkat reporter cells showed that these cells were not suited in the context of our CAR platform.
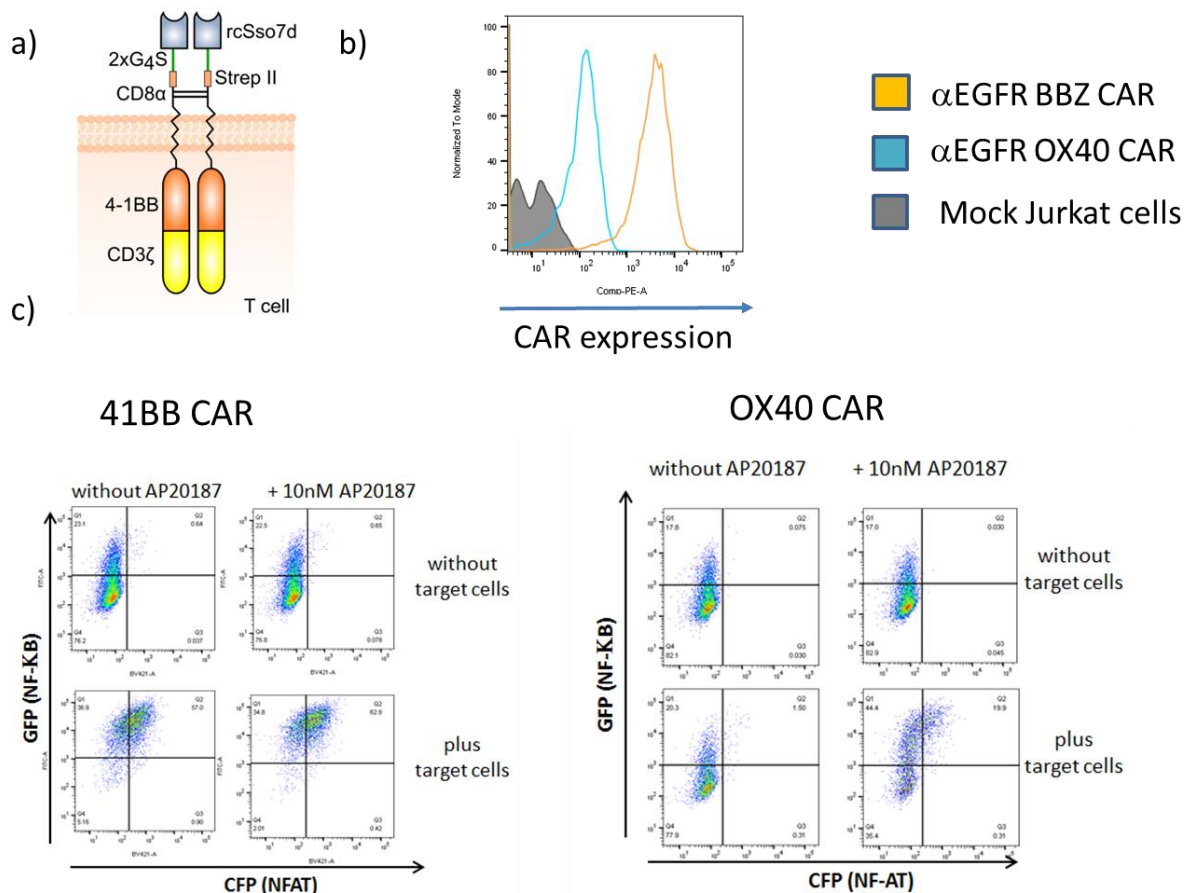
Figure 13: Testing of different co-stimulatory domains in dual reporter Jurkat cells

a) Configuration of the CAR constructs: Homodimerizable CAR carrying a reduced affinity $\alpha-$EGFR SSo7d binder. Co-stimulatory domains in this experiment included 4-1BB, OX40, ICOS and CD28; shown is the data for 4-1BB as well as OX40. Two identical CAR chains were dimerized with a B/B homodimerizer in order to generate avidity. Illustration by Benjamin Salzer.

b) Expression of the OX40 and 4-1BB CARs compared to Jurkat cells bearing no construct: Grey filled curve indicates Jurkat cells expressing no construct. Blue line shows Jurkat cells expressing the OX40 CAR, orange line indicated expression of the 4-1BB CAR. CARs were stained with a Strep II specific antibody.

c) Scatterplots showing the activation of dual reporter Jurkat cells after 19 hours of incubation: X-axis shows NFAT activation as measured by CFP expression. Y-axis shows NF-κB activation by GFP expression. Conditions included co-culture with or without hEGFRt positive target cells. 10 nM B/B homodimerizer AP20187 was added as indicated. Dual reporter effector cells as well as target cells were electroporated with 5 μg of mRNA in a volume of 100 μL (with max. 10 million cells) one day before the experiment. Shown are plots for the OX40 and 4-1BB CARs. The latter is representative for other co-stimulatory domains. The experiment was only carried out once.

4.5 Influence of different co-stimulatory domains on efficacy and specificity

Since evaluation of the function of different co-stimulatory domains in our avidity-dependent CAR was not possible with 2PR Jurkat reporter cells, the experiments were repeated in primary T cells. Again, we tested CARs with co-stimulatory domains derived from 4-1BB, ICOS, OX40, CD28, and this time additionally CD2. Shown in Figure 14a are the expression levels of the various CAR constructs from three independent

experiments. All co-stimulatory domains save for CD28 resulted in low to medium background lysis and enhanced lysis upon addition of the B/B dimerizer (AP20187), i.e. in the dimeric state of the CARs. The CD28 CAR was not dependent on the presence of the B/B dimerizer, mediating high target lysis even without it. Addition of the dimerizer led to only a rather small increase in target cell lysis.

The same trends in T cell activation were observed again when assayed by cytokine production (IFN-γ), albeit differences between conditions with and without dimerizer were less pronounced. However, once again the CD28 seemed to trigger the strongest activation by far.

Modelling of the avidity dependent CARs, as was carried out by Benjamin Salzer in the group of Omer Dushek at the University of Oxford, had shown that upon dimerization of the CAR by a small molecule, the amount of bound receptor on the cell surface does not increase significantly. However, the half-life time of the bound receptor complex will increase dramatically, which is what might lead to the increase in T cell activation observed experimentally (as well as in the model). CARs harboring co-stimulatory domains with fast activation kinetics might therefore be triggered even in a monomeric state. This would ultimately result in strong lysis even in the absence of the small molecule dimerizer, as is the case for the CD28 CAR. This is shown in Figure 15.
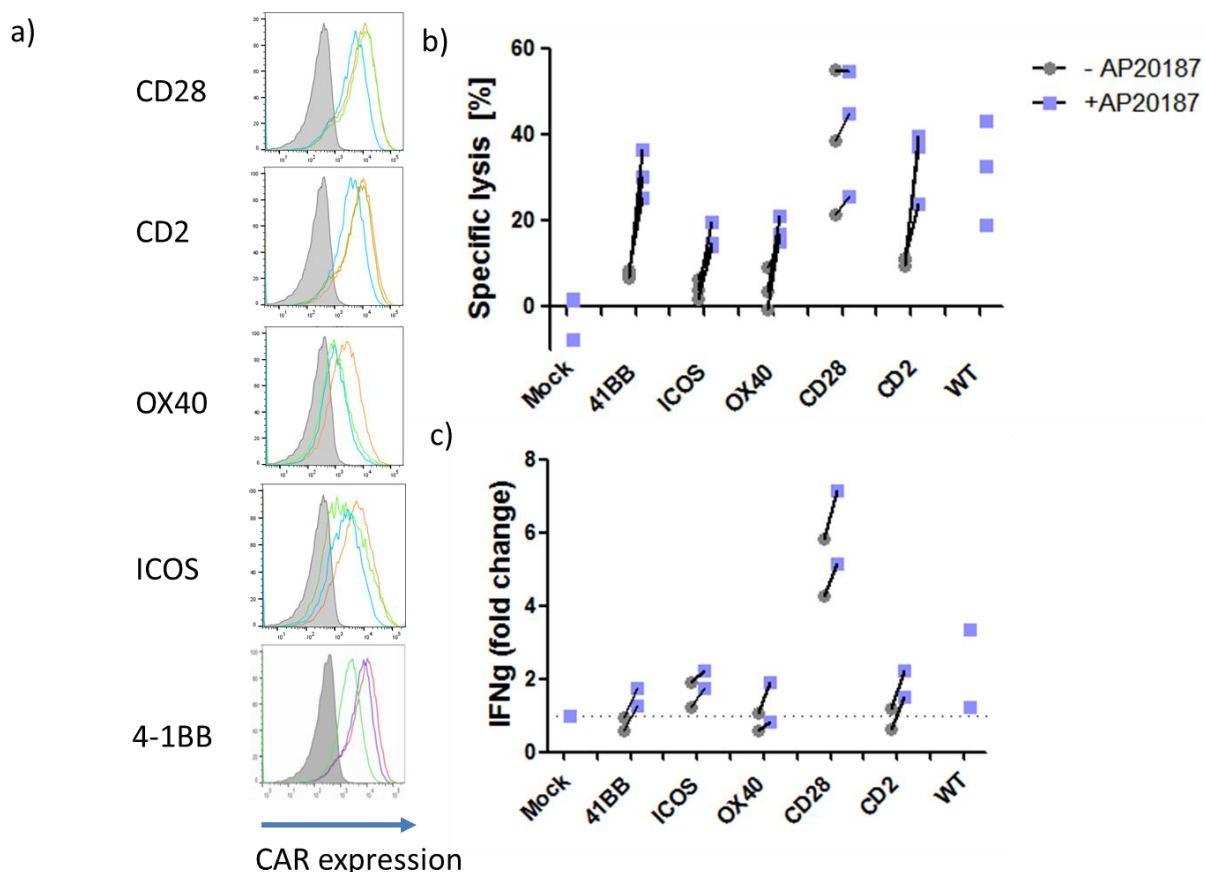
Figure 14: Testing of different co-stimulatory domains in primary T cells

a) Expressions of CAR constructs with different co-stimulatory domains: Grey filled curves are representative control cells not expressing a construct. Yellow, green and blue lines represent T cells from three different healthy donors and their expression levels of the indicated CAR construct. CARs were detected with a Strep II specific antibody.

b) Lytic activity of T cells expressing low-affinity CARs with different co-stimulatory domains: T cells were electroporated with 5 µg mRNA coding for each CAR construct. Target cells were electroporated with 5 µg of mRNA coding for hEGFRt. Shown are the results of three independent flow cytometry bases cytotoxicity assays.

c) Cytokine secretion of T cells expressing low-affinity CARs with different co-stimulatory domains: Supernatants from each cytotoxicity experiment were collected after 4 hours of incubation and stored at -80°C. Secretion of IFN-γ) was then evaluated by ELISA. Due to the high variation in cytokine secretion between donors, values were normalized to the background levels of T cells expressing no CAR.
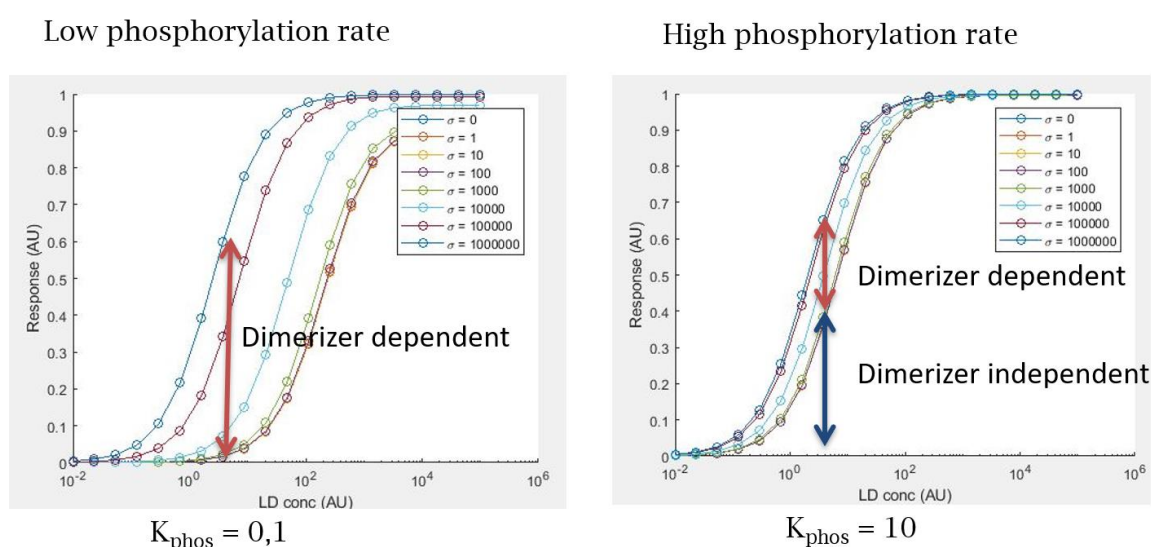
Figure 15: Results from modelling two different phosphorylation constants (K_{phos}) and thus different speeds of activation: Based on a mathematical model of an avidity switch CAR generated by Benjamin Salzer. The diagrams show that varying phosphorylation rate (K_{phos}) could explain the phenotypical differences between different CARs. "LD conc" on the x-axis denotes the concentration of the ligand or antigen, "Response" on the a-axis signifies the probability of T cell activation, as a consequence of receptor engagement. Sigma values shown in the plot are a proxy for the dimeric character of the receptor, with high values meaning a fully dimeric receptor and low values meaning an effectively monomeric receptor.

4.6 Leucine zipper CAR

Previous mouse model experiments showed the efficacy of the homodimerizable Sso7D anti-EGFR CAR *in vivo* (avidity based ON-switch CAR). The next step was to show the *in vivo*-function of an AND-gate CAR. A complication to this undertaking was that the A/C heterodimerizer (AP21967) is known to have a very low half-life *in vivo* of less than an hour [55]. This precluded an affinity-based AND-gate CAR from being tested in a murine model, as administering the substance to mice every hour would have been completely unfeasible. Since the main goal, however, was to merely evaluate the efficacy of an avidity-based AND-gate CAR in a mouse model, we instead built a constitutively active AND-gate CAR. For this purpose, we replaced the FKBP dmrA and dmrC domains in the previous CARs with leucine zipper RR and EE domains respectively, which bind each other with high affinity, forming heterodimers [75]. We hypothesized that this would in turn enable the

generation of a constitutively active AND-gate CAR, which should only be efficiently activated by target cells expressing both hEGFRt and hHER2t. Figure 16a shows the architecture of this leucine zipper AND-gate CAR.

Displayed in Figure 16c is the cytotoxicity assay data from five independent experiments (and three different donors respectively). T cells without CAR and T cells transiently transfected by mRNA electroporation to express both leucine zipper CAR chains (77% were double positive, see Figure 16b were co-cultured with hEGFRt^{pos} Jurkat cells, hHER2t^{pos} Jurkat cells (both of them single positive) and hEGFRt[pos]/hHER2t[pos] (double positive) Jurkat cells. T cells without CAR did not mediate disproportionate lysis of any of the target cell populations. Strikingly, T cells expressing the leucine zipper AND-gate CAR induced relatively high lysis of hEGFRt[pos]/hHER2t^{pos} Jurkat cells, but only low lysis of single antigen^{pos} Jurkat cells.

In addition to the cytotoxic activity, IFN-γ concentrations in the culture supernatants of the cytotoxicity assays were measured by ELISA (Figure 16d). Since the biological variation between donors was relatively high, values were normalized to mean levels secreted by T cells in contact with single antigen^{pos} target cells. Cytokine secretion was approximately 2.5-fold enhanced when comparing double positive to single positive target cells, again demonstrating the specificity of the leucine zipper AND-gate CAR.
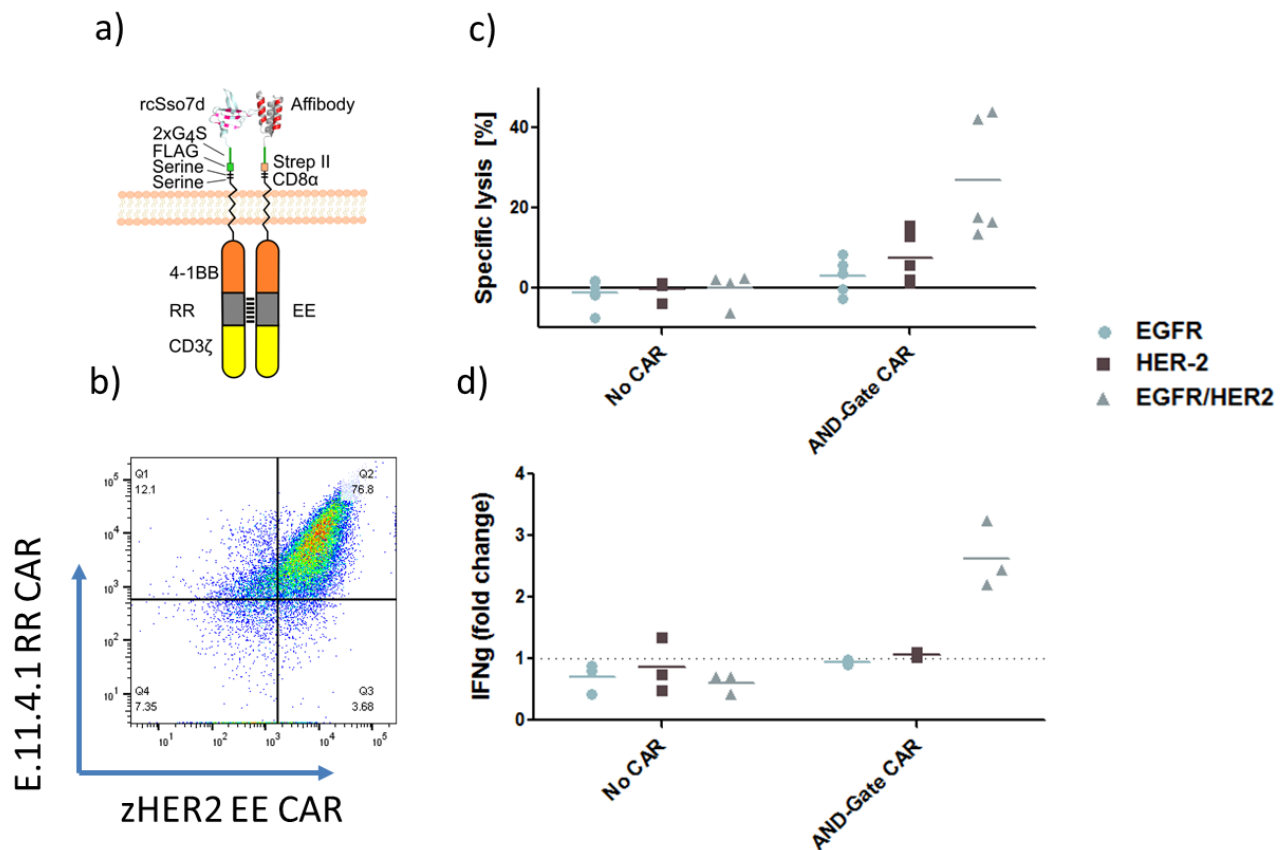
Figure 16: Constitutive AND-gate

a) Architecture of the leucine zipper AND-gate CAR: Two separate, similarly constructed chains, one including an Sso7d binder targeting hEGFR and a RR leucine zipper domain, the other chain comprising an affibody binder targeting hHER2. Both chains carry a 4-1BB co-stimulatory domain as well as a CD3ζ domain. Illustration by Benjamin Salzer.

b) Representative scatterplot showing the expressions of the E.11.4.1 RR and the zHER2 EE CAR chains: E.11.4.1 RR chain was stained with a Strep II specific antibody, the zHER2 EE chain was stained with a Flag specific antibody.

c) Functional testing of the RR/EE leucine zipper CAR by flow cytometry-based cytotoxicity assay: T cells were electroporated with 5 µg of mRNA for both chains. Target cells were Jurkat cells expressing either hEGFRt, hHER2t or both antigens (5 µg of mRNA per target antigen). Cells were co-cultured for 4 hours and specific lysis was evaluated by flow cytometry. Five experiments obtained with three different donors are shown.

d) Functionality of the constitutive AND-gate CAR assessed by cytokine secretion: Supernatants from each cytotoxicity experiment were collected after 4 hours of incubation and stored at -80°C. Cytokine secretion was then evaluated by IFN-γ ELISA. Due to the high variation in cytokine secretion between donors, values were normalized to average cytokine levels secreted by T cell co-cultured with single antigen^{pos} target cells. Three independent experiments with three different donors are shown.

The leucine zipper CAR was also tested in dual reporter Jurkat cells, as it allowed for more combinations of conditions to be examined (Figure 17). Jurkat cells expressing both chains displayed significant background activation of NF-κB signalling even without target cells, which could indicate strong tonic signalling induced by the CAR. However, reporter activation was strongest with Jurkat cells expressing both CAR chains in co-culture and target cells expressing both antigens (resulting in 36% NF-AT positive reporter cells). Nevertheless, reporter Jurkat cells expressing solely the RR leucine zipper CAR chain (carrying the hEGFR-specific binder) also showed relatively strong activation with 20.5% and 25.6% NF-AT positive cells in co-culture with hEGFRt[pos]/hHER2t[pos]- and hEGFRt[pos]- target cells, respectively. This indicates that in the absence of the EE leucine zipper CAR, without its intended partner, the RR leucine zipper CAR might tend to homodimerize, and thus recognize single antigen[pos] (hEGFR) target cells.
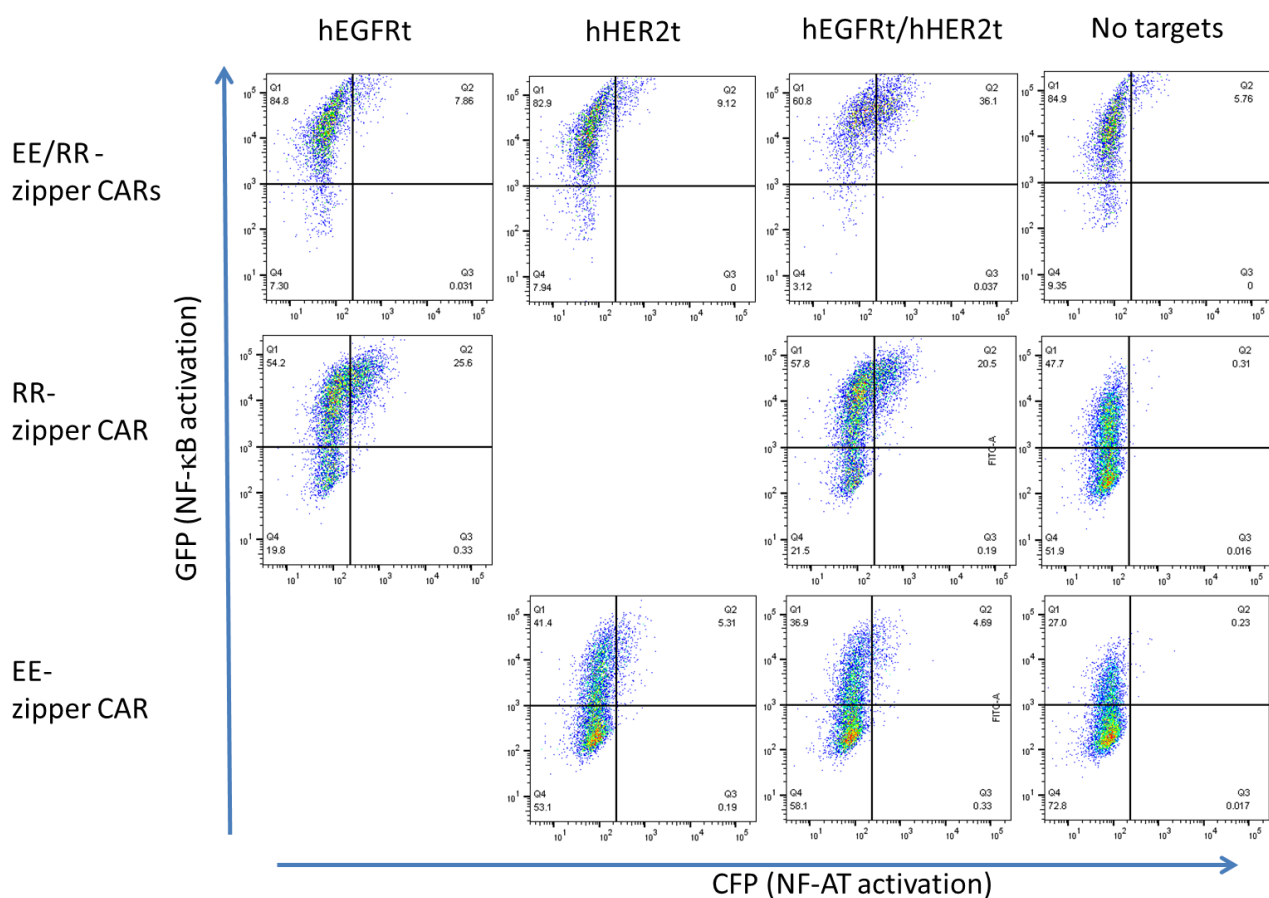
Figure 17: Evaluation of the RR/EE leucine zipper CAR in the dual reporter Jurkat cell line: Figure shows NF-AT and NF-κB activation in dual reporter cells expressing either the EE leucine zipper CAR, RR leucine zipper CAR or both chains. Dual reporter cells were electroporated with 5 µg of mRNA per chain. Target cells were prepared with 5 µg mRNA coding for hEGFRt, tHER2 or both. Cells were co-cultivated as indicated in the diagram for 19 hours and dual reporter activation was measured by flow cytometry. Experiment was carried out only once.

4.7 Identification of antigens suited for AND-gate CAR targeting of OS

4.7.1 Analysis of antigen expression in OS cell lines

As was discussed in the introduction, no significant improvements to treatment outcomes for OS have been achieved over the last decades, with survival rates for certain patient groups remaining especially low. Therefore, a potent and safe CAR T cell therapy would be highly beneficial for high risk OS patients. The goal of the second part of this work therefore was the identification of potential target antigens for CAR T cell therapy for OS. For this subproject we worked closely with Konstantin Byrgazov, who kindly provided a panel of 8 OS cell lines (HOS, U2OS, SaOS2, STA-OS-5, STA-OS-3, STA-OS-1, MG63, CAL72). We were aware that ultimately a high throughput *in silico* approach would most likely be necessary, in order to find meaningful combinations of antigens, which would satisfy both, the requirement of high expression, as well as the requirement of high tumor specificity. However, we concluded that the verification of the expression of potentially relevant markers in OS cell lines would be useful for the interpretation of finding in the subsequent *in silico* identification of potential OS target antigens. Therefore, the markers CD13, CD29, GD2, MDR-1 and PDL-1 were chosen based on literature indicating their relevance to OS [76], [77], [78].

The expression of all markers was analysed by staining with directly PE labelled antibodies. Median fluorescence intensities were used in order to approximate the number of molecules per cell via a PE bead calibration curve (PE Phycoerythrin Fluorescence Quantitation Kit, BD Biosciences). The histogram overlays in Figure 18 show the expression of the markers CD13, CD29, GD2, MDR-1 and PDL-1 as well as the autofluorescence of each cell line. Figure 19 details the average numbers of molecules per cell for these antigens. MDR-1 is expressed at very low levels only. The expression levels of CD13 and PDL-1 is low to medium and highly heterogeneous between cell lines. GD2, which is considered a highly attractive target in OS, is very highly expressed in three out of the eight cell lines, however, the distribution is smeared across a very broad range. This would make GD2 only a suboptimal candidate as a target, given the fact that a substantial subpopulation would not express the marker at sufficient levels to be targeted by the CAR and thus be *a priori* resistant. Finally, CD29 is universally highly expressed on all tested cell lines. However, it is expressed also at varying intensities on organs such as the kidneys, urinary bladder, colon, and most importantly highly expressed on smooth muscle tissue.[4]

---

[4] www.proteinatlas.org, 19.06.2019
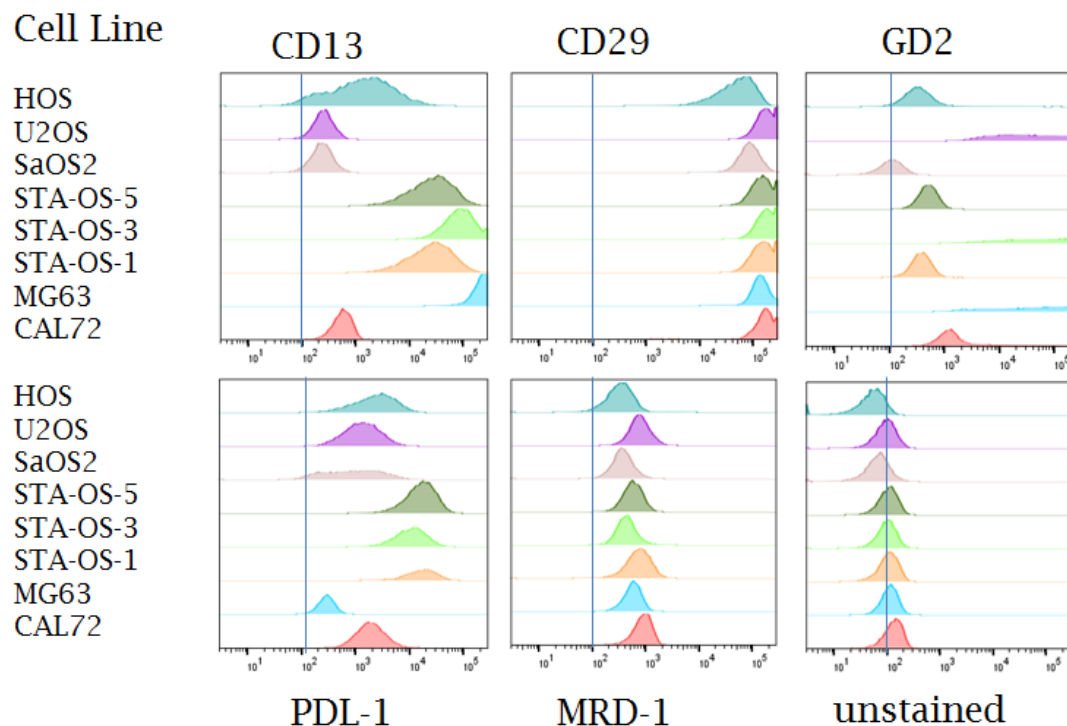
Figure 18: Flow cytometric analysis of the expression of the markers CD13, CD28, GD2, PDL-1 and MRD-1 on eight different human OS cell lines. Stainings of 100,000 cells each were carried out with the amount of antibody recommended by the manufacturer (see materials and methods). Cell lines were provided to us by Konstantin Byrgazov. STA-OS-1,2 and 5 are cell lines established in house at the CCRI. A line is displayed at an intensity of 10^2 for reference.
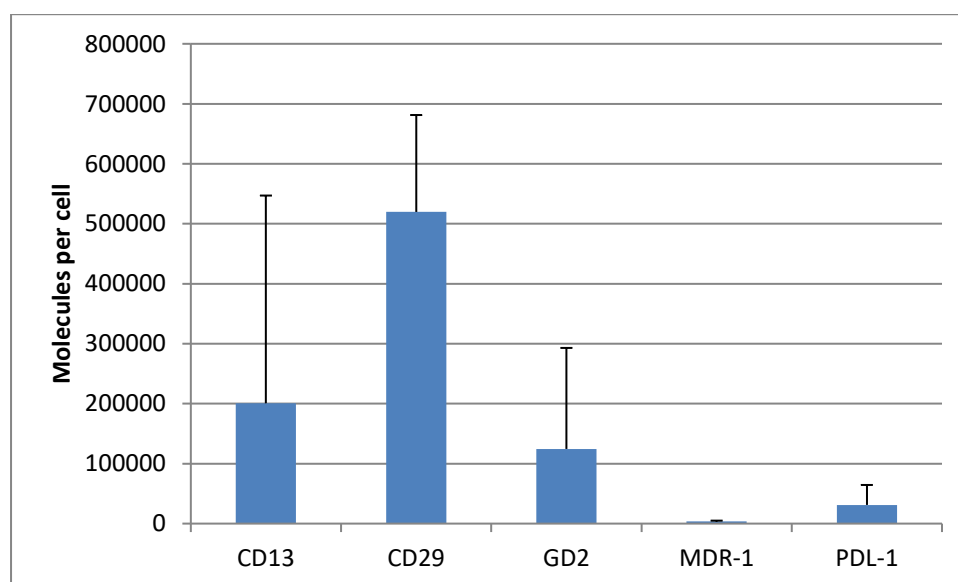
Figure 19: Surface expression of the investigated markers on OS cell lines: Shown are averages of molecules per cell from the eight cell lines listed above. Error bars indicate standard deviations. Error bars indicate standard deviation.

4.7.2 *In silico* analysis of antigen expression for the identification of potential markers and combinations of markers for specific targeting of OS

4.7.2.1 Quality control and exploratory data analysis

In a first step, the quality of our utilized data had to be assessed. An obvious weakness of our approach was that the datasets included in our analysis came from different sequencing centers. That is, samples were sequenced on different machines and therefore batch effects most likely come into play [79]. Moreover, we did not have a good option to assess or eliminate these batch effects, as none of the samples were analysed in more than one of the sequencing facilities which prevented the comparison and hence the calculation of these effects. We do think, however, that these batch effects would not significantly disturb our analysis, since in our case only large differences in expression levels are of interest. For quality control purposes of the data, a principal component analysis (PCA) was carried out. Shown in Figure 20 are PC1 (principle components) and PC2 of all the aggregated data. The major outliers in this representation are the testis (bottom right in pink), which is not entirely unexpected as testis express a large number of tissue specific genes [80]. In comparison all the other samples seem to cluster around the same center in the directions of PC1 and PC2. For a more detailed picture we thus also analysed PC3 versus PC4 (Figure 21). While there is appreciable overlap between tissues, samples from the same tissue generally cluster together. The OS samples form their own relatively distinguished cluster (blue ellipse on the lower right), which would be expected both due to biological variation as well as potential technical variation (batch effects). Overall, we concluded that there were no major concerns regarding quality of any of the sequencing data included in our search. Nevertheless, due to the sheer number of samples and groups it becomes relatively difficult to visualize the data conclusively without losing information to visual clutter.
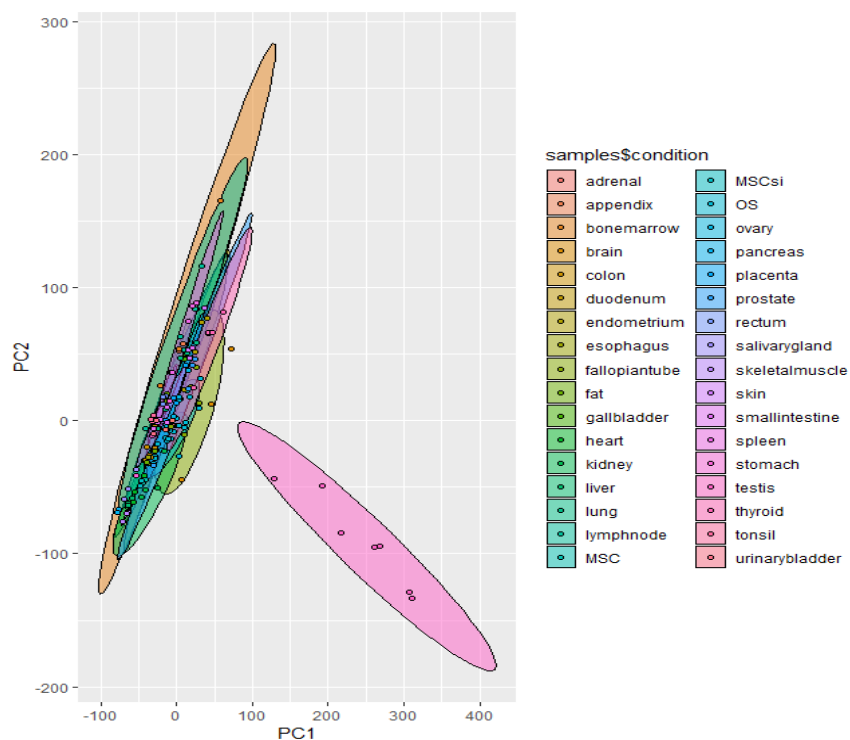
Figure 20: Principal component analysis including all samples used in the analysis: Principal components 1 and 2 are shown. Graphic was produced with ggplot2 for R.
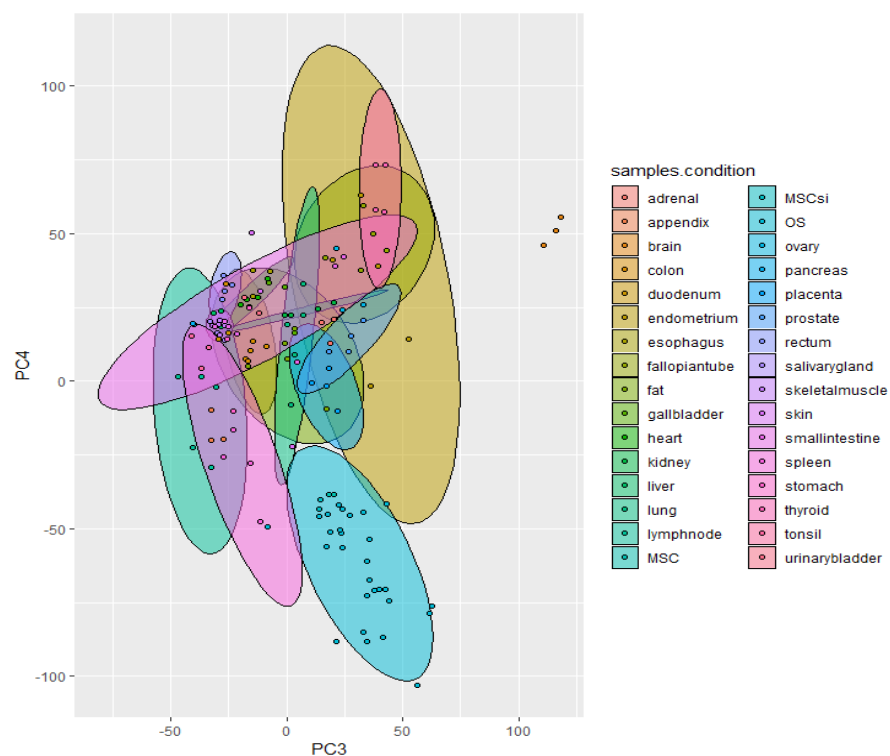

Figure 21: PCA analysis of samples excluding testis: Principal components 3 and 4 are shown. Graph was created with ggplot2.

4.7.2.2 Differential expression analysis of single genes

We made the assumption, that a CAR would approximately need a 100-fold difference in expression of a surface marker between cancer and healthy tissue in order to recognize the former as positive and the latter as negative (thus leading to effective discrimination of these tissues). Thus, we decided to search for genes that were overexpressed in OS with a log2 fold change value of > 6.5 (i.e. > ~90.5-fold change) when compared to a certain healthy tissue. In order to completely avoid on target/off tumor toxicities of a CAR, this condition would have to be fulfilled for all tissues in the human body. Whereas it is very unlikely that a single antigen is overexpressed at such high levels in all healthy tissues, it is much more realistic that the combination of two antigens fulfils this condition. In other words, we hypothesized that two markers, which are not tumor specific on their own, can be combined into a tumor specific pair of antigens.

Surprisingly, in initial screenings considering all genes, not only the genes coding for surface proteins, we were able to identify five genes that were overexpressed in OS when compared to all other tissues in our databank (Table 10). Two of those genes, PANX3 and IFITM5 coded for surface proteins (green rows), AMBN and COL2A1 coded for secretory proteins (light blue rows) and one (SP7) for an intracellular transcription factor.

Table 10: **Candidate genes (surface and other) that are overexpressed in OS compared to all healthy tissues:** The additional information, that is shown, is from the Human Protein Atlas.

EnsDB identifier	Gene ID	Gene Name	Information (human protein atlas)
ENSG00000139219	COL2A1	Collagen type II alpha 1 chain	Cancer-related genes, Disease related genes
ENSG00000154143	PANX3	Pannexin 3	Transporters
ENSG00000178522	AMBN	Ameloblastin	Disease related genes
ENSG00000170374	SP7	Sp7 transcription factor	Disease related genes, Transcription factors
ENSG00000206013	IFITM5	Interferon induced transmembrane protein 5	Disease related genes

In order to get a broader picture, we varied the cut-off for overexpressed genes between a log2 fold change of 6.5 and 2. Additionally, we also varied the number tissues that a given gene would have to discriminate OS against, as to receive a matrix of counts (see Table 11). At a log2 fold change cut-off of 6.5, with the requirement of full discrimination against 31 healthy tissues, we were left with 9 candidate genes. To our surprise the number of markers distinguishing OS from all heathy tissues increased only to 54 when going as low as a cut-off of 2, meaning only a 4-fold difference in gene expression versus healthy tissues.

Table 11: **Distribution of the number of specific markers over variable log2 fold thresholds as well as well as differential expression versus a variable number of tissues:** This analysis did not include osteoblast as well as mesenchymal stem cell samples

Overexpression compared to n tissues	log2 fold overexpression threshhold					
	6.5	6	5	4	3	2
31	9	11	15	19	25	54
30	14	20	25	38	55	110
25	37	45	83	123	234	434
20	65	79	139	259	498	931
15	105	140	253	466	929	1778

Since the expression level of the targeted marker is a major important factor for the efficacy of the CAR, we evaluated transcript abundance of markers IFITM5 and PANX3, the only surface markers with log2 fold overexpression of 6.5, in individual OS samples with DESeq2. Figure 22 shows normalized counts of PANX3 and IFITM5 in all OS samples plus three OS cell lines and healthy tissues. Both markers are highly expressed in almost all OS samples of both primary as well as metastatic origin. Strikingly, OS cell lines express neither marker.

When PANX3 and IFITM5 are expressed in healthy tissues, the levels are only very low; in most cases both transcripts are completely absent. This is also the case for osteoblast and mesenchymal stem cells, which would be expected to be most similar to OS.

a) PANX3
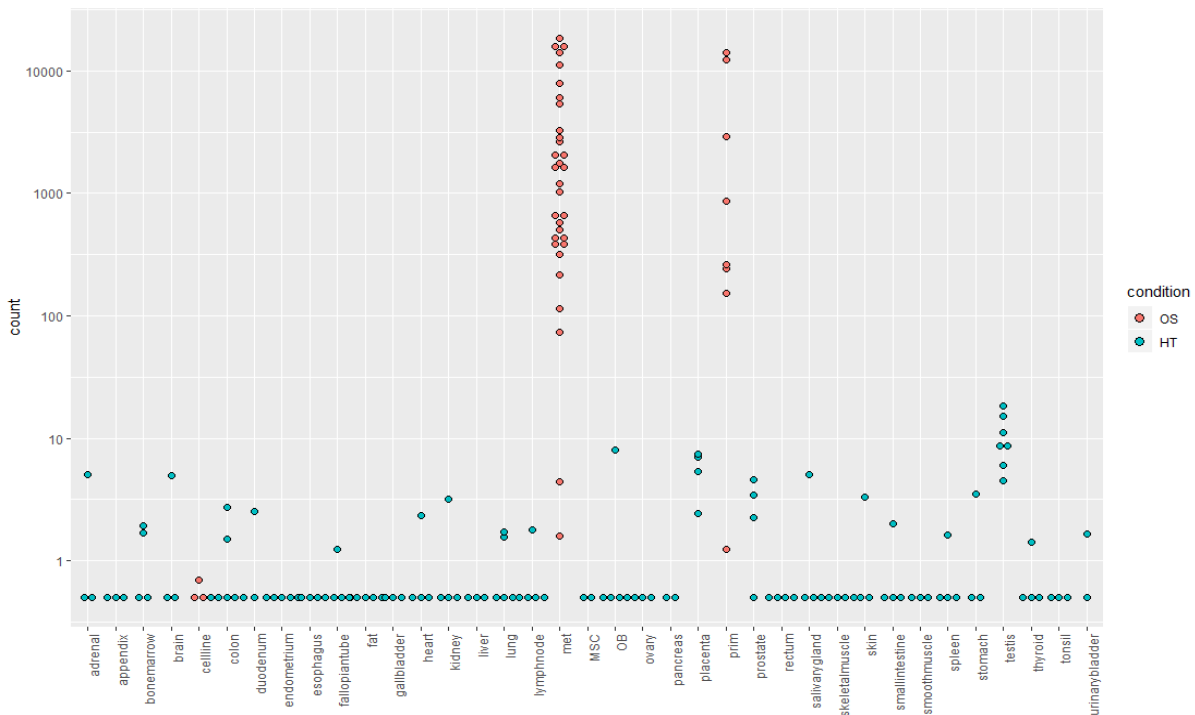
b) IFITM5
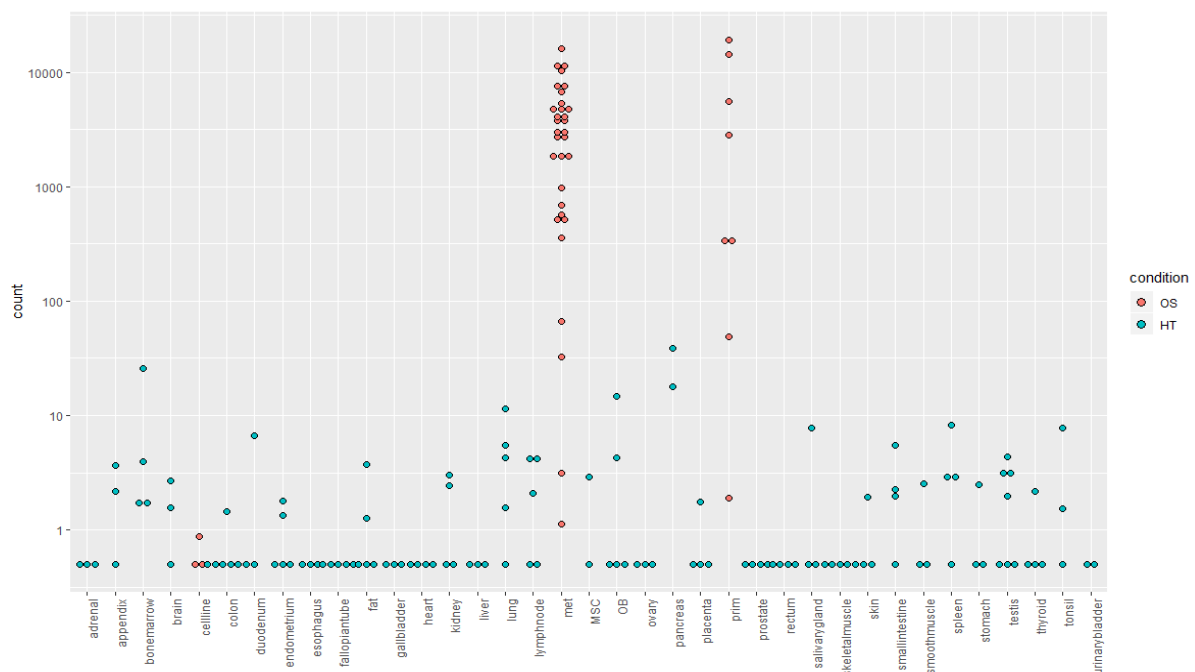
Figure 22: Expression levels of markers PANX3 and IFITM5: Signifiers on the x-axis denote the different healthy tissues as well as OS samples (primary, metastatic as well as three cell lines). "count" on the y-axis is a measure for transcript abundance generated by DESeq2, which normalizes for library size and thus allows for comparison on gene expression levels between samples (within the category of a certain gene). Comparisons between genes are not valid, however, as gene (transcript) length is not accounted for. OS cell lines are negative for both markers, while most OS tissue samples show high expression of the two genes. Importantly, most healthy tissue samples also show no expression of either marker.

4.7.2.3 Search for tumor specific pairs of antigens

Next, we conducted a paired search, where every surface protein was paired with every other surface protein (described in more detail in Methods "paired search"). The condition for every such combination was the same as for single markers: a given combination should be able to discriminate OS against every single healthy tissue in our database at a given log2 fold change level and *P* value. In order to score a hit against a particular healthy tissue one of the two markers of a pair being overexpressed was sufficient. Interestingly, apart from the two markers PANX3 and IFITM5, at a log2 fold change value of 6.5 no pairs where found that were able discriminate OS against every healthy tissue. We therefore lowered the cutoff to 2^5 and were able to identify 22 unique pairs of markers (see Table 12). Recurring proteins amongst the 22 pairs were CDH15, SLC8A3, FAT3 as well as LRRC15. Many of the candidates found in this analysis were also found in the top 100 ranked single markers (for ranking see methods 3.5.3 Obtaining tumor specific markers). Important note: At the time of writing this thesis we had not controlled for multiple testing with regards to pair formation, which makes false positives likely.

Table 12: Combinations of markers that are able to discriminate OS from all healthy tissues including osteoblasts and mesenchymal stem cells

Marker combinations
ALPL/CDH15
SNORC/LRRC15
CDH15/CNMD
CDH15/GLRA3
CDH15/IER3
CDH15/LRRC15
CDH15/OCSTAMP
CDH15/TNFSF11
CNMD/CTSK
CNMD/LRRC15
FAT3/LRRC15
FAT3/OCSTAMP
FAT3/PIGY
LRRC15/PTH1R
LRRC15/SLC36A2
LRRC15/SLC8A3
OCSTAMP/PIGY
OCSTAMP/SLC8A3
PHEX/PIGY
SLAMF9/SLC8A3
SLC8A3/TNFSF11
SLC8A3/TRPV4

5. Discussion

Our group previously described a CAR system implementing both ON-switch and AND-gate function. These are measures to increase safety of CAR T cell therapies. Both features are based on an effective affinity gain through bivalent binding, i.e. avidity. It was shown that, below a certain affinity threshold, monovalent interaction between CAR and antigen was insufficient for full T cell activation. A monomeric anti-EGFR CAR with a K_D value of 13 nM could effectively lyse antigen^{pos} target cells, while a monomeric CAR with an affinity of approximately 800 nM was unable to do so. A dimeric reduced affinity CAR, however, was fully functional due to avidity contributions to apparent affinity. This behavior could be utilized to implement both AND-gate, as well as ON-switch functions, by building a CAR consisting of two monomeric chains, each comprising a heterodimerization domain and a reduced affinity binder targeted against antigens EGFR and HER2, respectively (AND-gate function). Conditional dimerization via the small molecule AP21967 acted as an ON-switch.

Here we showed a variety of different results, all of them regarding the optimization and potential applications of the avidity-based CAR: The affibody anti-HER2 binder utilized in the AND-gate, next to the EGFR specific binder, was biochemically characterized by SPR. Furthermore, a variety of alternative co-stimulatory domains were tested in double reporter Jurkat cells as well as in primary T cells. Additionally, we generated and functionally tested a novel CAR implementing a constitutive AND-gate function, based on drug-independent heterodimerization via leucine zipper domains. Lastly, we identified possible target antigens and target antigen combinations, which are highly specific to OS.

CARs harboring two different mutant variants (R10A and R32A) of the HER2 specific affibody binders were functionally shown to be dependent on the presence of the small molecule homodimerizer AP20187. To biochemically characterize these mutant versions and the wild type binder, these proteins were recombinantly expressed as fusion proteins to sfGFP. Since affibodies are very small proteins, the increase of the molecular weight by fusion to sfGFP enhanced the binders' properties for SPR analysis. This is due to the fact that in SPR the detected signal is proportional to the mass of bound material on the sensor chip. In these experiments, we determined a K_D value of approximately 23 nM for the WT binder. The R32A and R10A variants' K_D values were 285 nM and 639 nM, respectively. As we had suspected these values exhibited striking parallels to the affinity ranges of the anti-EGFR SSo7D binders. This is especially interesting as the CAR is not only directed against a different antigen but also harbors a completely different binder scaffold, this being an affibody instead of an Sso7D binder: Affibodies are artificial proteins derived from Z domain in Protein A, which naturally occurs in the cell wall of *Staphylococcus aureus.* Structurally, it consists of a three α-helix bundle which mediate specific antigen binding [81]. Sso7d in contrast is a binding scaffold originating from *Sulfolobus solfataricus* a hyperthermophilic archeon and consists mainly of β-sheets [82].

SPR measurements showed that the largest contribution to the overall lower total affinity of the mutated binder variants stemmed from a much faster dissociation rate, as opposed to a slower association rate. As discussed before, mathematical models by Benjamin Salzer suggested that the duration of individual interactions between CAR and antigen could be a critical parameter for T cell activation. The SPR data fit in line with this hypothesis, as a much faster dissociation rate would certainly mean a reduced half-life of the interaction between CAR and antigen. Overall, these findings show that it is possible to build avidity based AND-gates for CAR T cell therapy with reduced affinity binders of different types and origins. Additionally, they

suggest that a certain affinity threshold, below which monomeric CARs can no longer efficiently trigger a T cell response, might be relatively similar irrespective of binder and antigen structure.

CARs previously built by our group always comprised a 4-1BB co-stimulatory domain. One of this work's aim was to verify whether avidity based AND-gate CARs could function with co-stimulatory domains other than the initially used 4-1BB, and if so, whether improvements in specificity and efficacy, i.e. greater differences between monovalent and bivalent binding, could thereby be achieved. While there is a lot of overlap in function and downstream targets between various co-stimulatory domains in the context of CARs, there are some vital differences as well, which promise to offer a lot of room for context dependent optimization of CARs. CD28 CARs, for example, have been shown *in vivo* to initially lead to enhanced T cell expansion and cytotoxic activity compared to their 4-1BB counterparts. 4-1BB on the other hand seemed to be superior in terms of CAR T cells' long-term persistence, which could lead to a longer progression-free survival, as observed in patients with B-ALL [83]. Additionally, the positioning of the co-stimulatory domain within the CAR-endodomain can have effects of their efficacy as well [84].

To start out, we therefore built a panel of CARs comprising a reduced affinity anti-EGFR binder, a CD3ζ domain and the co-stimulatory domains ICOS, OX40 and CD28 in addition to the already existing 4-1BB CAR. In testing these CARs, we intended to utilize a dual reporter Jurkat cell line. As discussed, this platform promises various advantages over primary T cells: Firstly, the cell line eliminates the time-consuming and costly step of cultivating primary T cells, while being potentially always available, as cell lines can be continuously cultured. Primary T cells on the other hand, can only be used within a defined time frame after thawing and have only a limited potential for expansion. Lastly, Jurkat cells offer the benefit of having superior protein expression characteristics; hence they enable testing also of CAR constructs with otherwise insufficient expression in primary T cells.

In cytotoxicity experiments with primary T cells, our group showed the dependence of a reduced affinity CAR harboring a 4-1BB domain on the presence of the small molecule dimerizer AP20187. Contrary to these findings, the dual reporter cell line did not exhibit differences in NF-κB and NF-AT signaling with or without AP20187. This was despite the fact, that we tested a variety of different conditions, ranging from antigen density on target cells, CAR density on reporter cells, different time points from one hour up to 48 hours, to varying effector target ratios, as to exclude artefacts. A dependence on the dimerizers could ultimately only be observed with a CAR comprising an OX40 co-stimulatory domain.

The panel of constructed CARs (with the addition of a CD2 CAR) was therefore tested in primary T cells by measure of cytotoxicity assays as well as IFN-γ ELISA. Here, CARs with OX40, ICOS, CD2 and again 4-1BB co-stimulatory domains did exhibit strong dependence on the presence of AP20187. Between these CARs no co-stimulatory domain was conclusively superior in terms of efficacy or specificity (although ICOS seemed to induce the lowest background lysis). The CD28 CAR mediated the strongest T cell activation (measured by target cell lysis and cytokine secretion), however, it did so even without the addition of the small molecule dimerizer. The reasons for this remain unclear so far, however, we consider two possible explanations: A mostly monomeric state of the CAR is a requirement for it to be inactive without the small molecule dimerizer. CAR dimerization via an interaction between the intracellular CD28 domains could therefore eliminate its dependence of the dimerizer altogether. Indeed full length CD28 occurs as a natural homodimer [85]. Moreover, recent findings show that CD28/CD3ζ CARs can interact with endogenous CD28. This interaction could be mediated by the growth factor receptor-bound protein 2 (GRB2), which itself is a homodimeric

protein [86], [87]. GRB2 might therefore directly dimerize two CD28/CD3ζ CAR chains, or crosslink them via interaction with endogenous CD28, which would also allow for oligomerization of the CAR.

Secondly, we consider the possibility of faster activation kinetics when compared to a 4-1BB CAR, the influence of which we tested in a mathematical model. In our model we showed that a faster phosphorylation rate of CD28, when compared to other co-stimulatory domains, could indeed lead to T cell activation even with a monomeric CAR, similarly to what was observed experimentally. Interestingly, there is evidence for a faster triggering of CD28 CARs: Salter and colleagues demonstrated that CD28 CARs induced faster and larger changes in downstream protein phosphorylation than 4-1BB CARs did [37].

Overall, the question of the optimal form of co-stimulation is still inconclusive. Some evidence points towards the combination of domains, in the form of third generation CARs, more specifically towards the combination of 4-1BB with either ICOS or CD28, for optimum efficacy and CAR T cell persistence [88], [89]. While our results suggest that CD28 is not fit for use in our avidity-based CAR, combinations of other co-stimulatory domains in the form of third generation CARs could be considered.

The previously engineered AND-gate CAR relies on heterodimerization by AP21967, which is not stable *in vivo* [55]. Thus, for *in vivo* testing a different method of dimerization was needed. We replaced the FKBP heterodimerization domains in our AND-gate CAR with two complementary leucine zipper domains, which can facilitate the constitutive heterodimerization of the individual CAR chains [75]. Both chains were well expressed in primary T cells transiently transfected with mRNA. The CAR mediated high specific lysis of hEGFRt[pos]/hHER2t[pos] (double positive) target cells by T cells, while inducing only low levels of lysis amongst single antigen^{pos} target cells. We concluded that this CAR could therefore enable testing of an avidity-based AND-gate *in vivo.* Additionally, these results showed that CARs comprising different types of heterodimerization domains can be used to construct an avidity-based AND-gate. What makes the leucine zippers all the more attractive, is that they are derived from human B-ZIP proteins und hence are unlikely to be immunogenic [75]. Overall this clearly demonstrates the flexibility and modularity of our CAR platform, as it is functional with different binder scaffolds, different co-stimulatory domains, as well as different dimerization domains.

The last part of this work dealt with establishing a pipeline for the search of tumor surface antigens. While the main focus was placed on OS, this approach could be generalized to other malignancies as well. A database of healthy tissues was built for this purpose from data publicly available from the Human Protein Atlas, together with data from human mesenchymal stem cells and healthy osteoblasts, which both are potential progenitors of OS. OS samples were obtained from the INFORM registry. Expression levels of genes in OS were compared to every tissue in the database utilizing DESeq2. We then filtered for markers, or pairs of markers, that would be able to discriminate the bulk of OS samples from all healthy tissues in our database. In addition to a filtering approach, we employed a ranking based approach to test the stability of the results. Interestingly, in all of the results the two individual markers PANX3 as well as IFITM5 turned out to be the top hits, being the only two single markers able to differentiate OS from every single healthy tissue in our analysis. At this point, it is important to state that OS is a neoplasm of the bone-forming tissue, originating from a mesenchymal lineage. It is yet unclear from which cell type the disease originates precisely, however there is evidence for both mesenchymal stem cells themselves, as well as committed osteoblasts. Thus, it is possible that OS can arise at any point in the differentiation process from the stem cell to the committed osteoblast [65], [90]. Both IFITM5 and PANX3 are proteins involved in bone and cartilage formation or the development of relevant tissues/cell types, which lends some credence to our approach [91], [92], [93]. The validity of our screening approach is

further supported by the fact that all of the other top-ranked hits shown in Table 10 are matrix proteins, or matrix-associated proteins, important for building cartilage and osteoid matrix, the latter being a characteristic of OS. Another top ranked OS marker which is SP7, a transcription factor driving osteoblast and osteocyte differentiation, which also fits into this picture [94]. We therefore considered our approach to have at least some methodological validity, despite the previously discussed batch effects. Still, we are conscious of the weaknesses of our approach. Since the screening relies on data bases that do not cover all tissues in the human body and certainly also not all subtypes of relatively rare cells present in those tissues, it cannot be excluded that on-target/off-tumor toxicities might still pose a problem.

One example of this is the above mentioned expression of IFITM5 and PANX3 during differentiation of healthy chondrocytes and osteoblasts [91]. IFITM5, for example, has been characterized as an osteoblast specific protein which is relevant for bone mineralization [93]. Therefore, by targeting either marker in isolation, one would run the risk of on-target/off-tumor toxicities towards bone and/or cartilage forming cell types or their progenitors. This could be especially problematic in children still undergoing longitudinal bone growth. Thus, suitable second markers that are not expressed on any of the aforementioned tissues and cell types have to be found for IFITM5 and PANX3 to make them viable targets for CAR T cell therapy using our bispecific AND-gate CARs. Furthermore, we combined individual markers, resulting in 22 highly specific pairings. Although the level of minimum differential expression for these pairs was only 2^5-fold, this still shows that pair formation could greatly expand the pool of targeting opportunities (at least in OS). We consider this vital, as the further evaluation of potentially specific markers is, in any case, necessary and would likely lead to the exclusion of the majority of them. Such an evaluation process would have to address the following points: Our *in silico* analysis relies on RNA sequencing data from bulk tissue, that is, it remains to be determined how these data translate to protein expression levels and additionally how variable expression levels are between individual cells of the same tumor. Furthermore, it has to be confirmed that the protein in question is expressed on the cell surface and in case for pairs of markers, whether both proteins are expressed on the same cell, or only on different cell subtypes present in the same tissue. Interestingly, we could show that neither PANX3, nor IFITM5, were expressed in the analysed OS cell lines. This finding suggests that OS cell lines might be a very poor model for confirming potential OS targets on a protein level. For this purpose, tissue sections of tumor material should definitely be preferred.

Currently, there are multiple important caveats remaining, regarding our *in silico* approach. Future evaluation of the stability of our findings by utilizing and comparing different methods would therefore be beneficial. For example, for both mapping as well as calculating differential expressions, alternatives to the tools used by us, should be tested and the results compared. Instead of kallisto tools such as Salmon, Sailfish and Bowtie2 could be employed, while alternatives to DESeq2 exist in the form of edgeR and Limma-Voom. Another remaining issue is the one of multiple testing. Although DESeq2 automatically corrects for multiple testing with regards to all tested genes, we did not correct for multiple testing regarding different tissues or pairs. Especially in the case of pair formation (due to the sheer volume of screened pairs) it is therefore likely that at least some of the identified pairs are false positives. Before giving too much importance to these results the issue of multiple testing definitely has to be addressed.

After the outstanding success of CAR T cell therapy in the treatment of some hematological malignancies, efforts are being made to develop CARs for the treatment of solid tumors in hopes of replicating this achievement. However, current CAR T cell therapies for solid tumors still leave a lot to be desired, as a meta-analysis by Hou et al. 2018 only showed a pooled response rate of 9% in 262 patients from 22 different studies, in which a diverse set of markers such as HER2, EGFR, GPC3, VEGFR2, CE7R and others were targeted. The

trials show low to no efficacy and mainly focus on the tolerability of the therapy for the patient [69], [95]. Even if remissions are achieved, tumors do eventually relapse due to acquired or preexisting resistances or lacking CAR T cell persistence. Solid tumors, in comparison with hematological malignancies (such as B-ALL), have the added complication of low accessibility for CAR T cells as well as a suppressive tumor-microenvironment. In order to overcome these factors, more potent CAR treatments, meaning armored or otherwise stimulated CAR T cells, higher cell dosages or combination with immune checkpoint blockade, become paramount. Enhancing potency however, all the more, raises the question of safety and specificity. Thus, tools are required that allow a more fine-tuned discrimination of tumor cells from healthy tissues. Our group has laid out a blueprint for how this could be achieved, by creating monomeric CARs with reduced affinities and exploiting the avidity effect, which allows for implementation of AND-gate and ON-switch functions in CARs.

However, one major weakness of AND-gate CARs is the increased probability of tumors developing resistance towards the therapy through the mechanisms of antigen loss or epitope mutation. Resistances are best managed through combination therapy with different substances or agents, for which no common resistance mechanisms exist. This is due to the fact that the probability for one subclone simultaneously acquiring two independent resistance mutations, is much lower than acquiring resistance mutations sequentially [96], [97]. Thus, also for AND-gate CARs parallel targeting of further alternative antigens has to be considered, as it is being done in targeting B cell malignancies. There, CAR-T cells with OR-gate function, i.e., CAR T cells that recognize cells whether they express antigen A *or* antigen B (e.g., CD19 *or* CD22) are currently being clinically tested [98]. In the context of an AND-gate this means the following: Either CAR chain, of which both being triggered simultaneously is required for full T cell activation, can bind to and recognize more than one target antigen. One way of achieving this would be via multi-specific binders. Hereto, binder scaffolds are engineered to bind multiple epitopes with high specificity and affinity. Additionally, adaptor-based CARs could be utilized, where the CAR is targeted towards the tumor by soluble adaptor fragments carrying an antigen-specific binding domain, as well as a domain interacting with the CAR stump. A switching of targets mid therapy, as is discussed for this type of CAR in the literature, however, is definitely not preferred, as this would result in a higher probability of resistances arising as discussed above [54], [56], [96].

Summarizing, we were able to show that different binder scaffolds can be utilized in an avidity-based AND-gate and that the optimal affinity ranges for these different binders seem to be very similar. Moreover, we could show that a variety of co-stimulatory domains, save for CD28, can be used in CARs that exploit avidity. In our experiments, we addionally demonstrated that an avidity-based AND-gate CAR cannot only be based on small-molecule induced dimerization via FKBP domains, but also on constitutive dimerization via leucine zipper domains. Finally, we were able to identify a panel of specific surface markers (single markers and pairs) that could be used for specific targeting of OS by CAR T cells

6. Literature

[1]   S. Guedan, H. Calderon, A. D. Posey, and M. V. Maus, "Engineering and Design of Chimeric Antigen Receptors," *Mol. Ther. - Methods Clin. Dev.*, vol. 12, pp. 145–156, Mar. 2019.

[2]   D. T. Teachey *et al.*, "Identification of predictive biomarkers for cytokine release syndrome after chimeric antigen receptor T-cell therapy for acute lymphoblastic leukemia," *Cancer Discov.*, vol. 6, no. 6, pp. 664–679, 2016.

[3]   M. V Maus and C. H. June, "Making Better Chimeric Antigen Receptors for Adoptive T-cell Therapy," *Clin. Cancer Res.*, vol. 22, no. 8, pp. 1875–1884, Apr. 2016.

[4]   A. D. Fesnak, C. H. June, and B. L. Levine, "Engineered T cells: the promise and challenges of cancer immunotherapy," *Nat. Rev. Cancer*, vol. 16, no. 9, pp. 566–581, Sep. 2016.

[5]   G. Sa, "Cancer immunoediting: Integrating the role of immunity in cancer suppression and promotion," *Sci. Signal.*, vol. 331, no. March, p. 78, 2011.

[6]   D. Ribatti, "The concept of immune surveillance against tumors: The first theories," *Oncotarget*, vol. 8, no. 4, pp. 7175–7180, 2017.

[7]   Stutman O, "Tumor development after 3-methylcholanthrene in immunologically deficient athymic-nude mice," *Science (80-.).*, vol. 183, no. 4124, pp. 534–536, 1974.

[8]   G. P. Dunn, A. T. Bruce, H. Ikeda, L. J. Old, and R. D. Schreiber, "Cancer immunoediting: from immunosurveillance to tumor escape," *Nat. Immunol.*, vol. 3, no. 11, pp. 991–998, Nov. 2002.

[9]   M. D. Vesely, M. H. Kershaw, R. D. Schreiber, and M. J. Smyth, "Natural Innate and Adaptive Immunity to Cancer," *Annu. Rev. Immunol.*, vol. 29, no. 1, pp. 235–271, 2011.

[10]   A. S. Dighe, E. Richards, L. J. Old, and R. D. Schreiber, "Enhanced in vivo growth and resistance to rejection of tumor cells expressing dominant negative IFNγ receptors," *Immunity*, vol. 1, no. 6, pp. 447–456, 1994.

[11]   V. Shankaran *et al.*, "IFNγ, and lymphocytes prevent primary tumour development and shape tumour immunogenicity," *Nature*, vol. 410, no. 6832, pp. 1107–1111, 2001.

[12]   D. Mittal, M. M. Gubin, R. D. Schreiber, and M. J. Smyth, "New insights into cancer immunoediting and its three component phases—elimination, equilibrium and escape," *Curr. Opin. Immunol.*, vol. 27, pp. 16–25, Apr. 2014.

[13]   D. Hanahan and R. A. Weinberg, "Hallmarks of cancer: The next generation," *Cell*, vol. 144, no. 5, pp. 646–674, 2011.

[14]   S. Rafiq *et al.*, "Targeted delivery of a PD-1-blocking scFv by CAR-T cells enhances anti-tumor efficacy in vivo," *Nat. Biotechnol.*, vol. 36, no. 9, pp. 847–856, Oct. 2018.

[15]   O. O. Yeku, T. J. Purdon, M. Koneru, D. Spriggs, and R. J. Brentjens, "Armored CAR T cells enhance antitumor efficacy and overcome the tumor microenvironment," *Sci. Rep.*, vol. 7, no. 1, pp. 1–14, 2017.

[16]   R. Alam, "A BRIEF REVIEW OF THE IMMUNE SYSTEM," *Prim. Care Clin. Off. Pract.*, vol. 25, no. 4, pp. 727–738, Dec. 1998.

[17]   W. Hoffman, F. G. Lakkis, and G. Chalasani, "B cells, antibodies, and more," *Clin. J. Am. Soc. Nephrol.*, vol. 11, no. 1, pp. 137–154, 2016.

[18]   M. H. Andersen, D. Schrama, P. thor Straten, and J. C. Becker, "Cytotoxic T Cells," *J. Invest. Dermatol.*, vol. 126, no. 1, pp. 32–41, Jan. 2006.

[19]   R. V. Luckheeram, R. Zhou, A. D. Verma, and B. Xia, "CD4 +T cells: Differentiation and functions," *Clin. Dev. Immunol.*, vol. 2012, 2012.

[20]   M. H. Andersen, D. Schrama, P. thor Straten, and J. C. Becker, "Cytotoxic T Cells," *J. Invest. Dermatol.*, vol. 126, no. 1, pp. 32–41, Jan. 2006.

[21]   N. Kerkvliet and B. P. Lawrence, "Cytotoxic T Cells," in *Comprehensive Toxicology, Second Edition*, 2010.

[22]   D. L. Wagner *et al.*, "High prevalence of Streptococcus pyogenes Cas9-reactive T cells within the adult human population," *Nat. Med.*, vol. 25, no. 2, pp. 242–248, 2019.

[23]   S. Halle, O. Halle, and R. Förster, "Mechanisms and Dynamics of T Cell-Mediated Cytotoxicity In Vivo," *Trends Immunol.*, vol. 38, no. 6, pp. 432–443, Jun. 2017.

[24]   D. Chowdhury and J. Lieberman, "Death by a Thousand Cuts: Granzyme Pathways of Programmed Cell Death," *Annu. Rev. Immunol.*, vol. 26, no. 1, pp. 389–420, Apr. 2008.

[25]   B. Shang, Y. Liu, S. Jiang, and Y. Liu, "Prognostic value of tumor-infiltrating FoxP3+ regulatory T cells in cancers: a systematic review and meta-analysis," *Sci. Rep.*, vol. 5, no. 1, p. 15179, Dec. 2015.

[26]   T. Tanoue, K. Atarashi, and K. Honda, "Development and maintenance of intestinal regulatory T cells," *Nat. Rev. Immunol.*, vol. 16, no. 5, pp. 295–309, May 2016.

[27]   J. B. Alimonti, "Mechanisms of CD4+ T lymphocyte cell death in human immunodeficiency virus infection and AIDS," *J. Gen. Virol.*, vol. 84, no. 7, pp. 1649–1661, Jul. 2003.

[28]   K. W. Wucherpfennig, E. Gagnon, M. J. Call, E. S. Huseby, and M. E. Call, "Structural biology of the T-cell receptor: insights into receptor assembly, ligand recognition, and initiation of signaling.," *Cold Spring Harb. Perspect. Biol.*, vol. 2, no. 4, pp. 1–14, 2010.

[29]   J. E. Smith-Garvin, G. A. Koretzky, and M. S. Jordan, "T Cell Activation," *Annu. Rev. Immunol.*, vol. 27, no. 1, pp. 591–619, Apr. 2009.

[30]   N. Hosoda, H. Miura, S. Takanashi, H. Shirai, and W. Sunaoshi, "V(D)J Recombination: Mechanism, Errors, and Fidelity," in *Mobile DNA III*, vol. 45, no. 2, American Society of Microbiology, 2014, pp. 313–324.

[31]   T. W. Mak and M. E. Saunders, "T Cell Activation," in *The Immune Response*, Elsevier, 2006, pp. 373–401.

[32]   P. A. Van Der Merwe and O. Dushek, "Mechanisms for T cell receptor triggering," *Nat. Rev. Immunol.*, vol. 11, no. 1, pp. 47–55, 2011.

[33]   T. Thaventhiran, "T cell Receptor Signal Transduction in T lymphocytes," *J. Clin. Cell. Immunol.*, vol. 01, no. S12, 2013.

[34]   G. Gaud, R. Lesourne, and P. E. Love, "Regulatory mechanisms in T cell receptor signalling," *Nat. Rev. Immunol.*, vol. 18, no. 8, pp. 485–497, Aug. 2018.

[35]   S. Goral, "The three-signal hypothesis of lymphocyte activation/targets for immunosuppression," *Dial. Transplant.*, vol. 40, no. 1, pp. 14–16, Jan. 2011.

[36]   R. H. Schwartz, "T CELL ANERGY," *Annu. Rev. Immunol.*, vol. 21, no. 1, pp. 305–334, Apr. 2003.

[37]   C. A. R. T. Cells *et al.*, "Phosphoproteomic analysis of chimeric antigen receptor signaling reveals kinetic and quantitative differences that affect cell function," *Sci. Signal.*, vol. 11, no. August, pp. 1–18, 2018.

[38]   A. H. Long *et al.*, "4-1BB costimulation ameliorates T cell exhaustion induced by tonic signaling of chimeric antigen receptors," *Nat. Med.*, vol. 21, no. 6, pp. 581–590, Jun. 2015.

[39]   Y. Kuwana *et al.*, "Expression of chimeric receptor composed of immunoglobulin-derived V resions and T-cell receptor-derived C regions," *Biochem. Biophys. Res. Commun.*, vol. 149, no. 3, pp. 960–968, Dec. 1987.

[40]   J. Buechner *et al.*, "Global Registration Trial of Efficacy and Safety of CTL019 in Pediatric and Young Adult Patients with Relapsed/Refractory (R/R) Acute Lymphoblastic Leukemia (ALL): Update to the Interim Analysis,"

Clin. Lymphoma Myeloma Leuk., vol. 17, pp. S263–S264, Sep. 2017.

[41] D. H. Yoon, M. J. Osborn, J. Tolar, and C. J. Kim, "Incorporation of immune checkpoint blockade into chimeric antigen receptor T cells (CAR-Ts): Combination or built-in CAR-T," *Int. J. Mol. Sci.*, vol. 19, no. 2, 2018.

[42] S. A. Richman *et al.*, "High-Affinity GD2-Specific CAR T Cells Induce Fatal Encephalitis in a Preclinical Neuroblastoma Model," *Cancer Immunol. Res.*, vol. 6, no. 1, pp. 36–46, Jan. 2018.

[43] M. M. D'Aloia, I. G. Zizzari, B. Sacchetti, L. Pierelli, and M. Alimandi, "CAR-T cells: The long and winding road to solid tumors review-article," *Cell Death Dis.*, vol. 9, no. 3, 2018.

[44] R. E. Voll, M. Herrmann, E. A. Roth, C. Stach, J. R. Kalden, and I. Girkontaite, "Immunosuppressive effects of apoptotic cells," *Nature*, vol. 390, no. 6658, pp. 350–351, Nov. 1997.

[45] J. J. L. P. Voss *et al.*, "Modulation of macrophage antitumor potential by apoptotic lymphoma cells," *Cell Death Differ.*, vol. 24, no. 6, pp. 971–983, 2017.

[46] V. L. Albaugh, C. Pinzon-Guzman, and A. Barbul, "Arginine-Dual roles as an onconutrient and immunonutrient," *J. Surg. Oncol.*, vol. 115, no. 3, pp. 273–280, Mar. 2017.

[47] D. S. Lind, "Arginine and Cancer," *J. Nutr.*, vol. 134, no. 10, p. 2837S–2841S, Oct. 2004.

[48] C. L. Bonifant, H. J. Jackson, R. J. Brentjens, and K. J. Curran, "Toxicity and management in CAR T-cell therapy," *Mol. Ther. - Oncolytics*, vol. 3, p. 16011, 2016.

[49] T. Giavridis, S. J. C. Van Der Stegen, J. Eyquem, M. Hamieh, A. Piersigilli, and M. Sadelain, "CAR T cell-induced cytokine release syndrome is mediated by macrophages and abated by IL-1 blockade letter," *Nat. Med.*, vol. 24, no. 6, pp. 731–738, 2018.

[50] M. Ruella *et al.*, "Induction of resistance to chimeric antigen receptor T cell therapy by transduction of a single leukemic B cell," *Nat. Med.*, vol. 24, no. 10, pp. 1499–1503, 2018.

[51] H. J. Jackson, S. Rafiq, and R. J. Brentjens, "Driving CAR T-cells forward," *Nat. Rev. Clin. Oncol.*, vol. 13, no. 6, pp. 370–383, 2016.

[52] T. Gargett and M. P. Brown, "The inducible caspase-9 suicide gene system as a 'safety switch' to limit on-target, off-tumor toxicities of chimeric antigen receptor T-cells," *Front. Pharmacol.*, vol. 5, no. OCT, pp. 1–7, 2014.

[53] A. Di Stasi *et al.*, "Inducible Apoptosis as a Safety Switch for Adoptive Cell Therapy," *N. Engl. J. Med.*, vol. 365, no. 18, pp. 1673–1683, Nov. 2011.

[54] W. A. Lim and C. H. June, "The Principles of Engineering Immune Cells to Treat Cancer," *Cell*, vol. 168, no. 4, pp. 724–740, 2017.

[55] C. Wu, K. T. Roybal, E. M. Puchner, J. Onuffer, and W. A. Lim, "Remote control of therapeutic T cells through a small molecule – gated chimeric receptor," vol. 350, no. 6258, 2015.

[56] J. H. Cho, J. J. Collins, and W. W. Wong, "Universal Chimeric Antigen Receptors for Multiplexed and Logical Control of T Cell Responses.," *Cell*, vol. 173, no. 6, p. 1426–1438.e11, 2018.

[57] D. M. Davies and J. Maher, "Gated chimeric antigen receptor T-cells: the next logical step in reducing toxicity?," *Transl. Cancer Res.*, vol. 5, no. S1, pp. S61–S65, Jun. 2016.

[58] K. T. Roybal *et al.*, "Precision Tumor Recognition by T Cells With Combinatorial Antigen-Sensing Circuits," *Cell*, vol. 164, no. 4, pp. 770–779, 2016.

[59] S. Sukumaran *et al.*, "Enhancing the Potency and Specificity of Engineered T Cells for Cancer Treatment," *Cancer Discov.*, vol. 8, no. 8, pp. 972–987, Aug. 2018.

[60] T. R. Mosmann, T. Yokota, R. Kastelein, S. M. Zurawski, N. Arai, and Y. Takebe, "Species-specificity of T cell

stimulating activities of IL 2 and BSF-1 (IL 4): comparison of normal and recombinant, mouse and human IL 2 and BSF-1 (IL 4).," *J. Immunol.*, vol. 138, no. 6, p. 1813 LP-1816, Mar. 1987.

[61]   A. Rongvaux *et al.*, "Human Hemato-Lymphoid System Mice: Current Use and Future Potential for Medicine," *Annu. Rev. Immunol.*, vol. 31, no. 1, pp. 635–674, Mar. 2013.

[62]   M. I. Love, W. Huber, and S. Anders, "Moderated estimation of fold change and dispersion for RNA-seq data with DESeq2," *Genome Biol.*, vol. 15, no. 12, pp. 1–21, 2014.

[63]   S. Jutz *et al.*, "Assessment of costimulation and coinhibition in a triple parameter T cell reporter line: Simultaneous measurement of NF-κB, NFAT and AP-1," *J. Immunol. Methods*, vol. 430, pp. 10–20, 2016.

[64]   R. A. Durfee, M. Mohammed, and H. H. Luu, "Review of Osteosarcoma and Current Management," *Rheumatol. Ther.*, vol. 3, no. 2, pp. 221–243, 2016.

[65]   A. Abarrategi *et al.*, "Osteosarcoma: Cells-of-Origin, Cancer stem cells, and targeted therapies," *Stem Cells Int.*, vol. 2016, 2016.

[66]   D. C. Allison *et al.*, "A meta-analysis of osteosarcoma outcomes in the modern medical era," *Sarcoma*, vol. 2012, no. March. 2012.

[67]   M. Overholtzer *et al.*, "The presence of p53 mutations in human osteosarcomas correlates with high levels of genomic instability," *Proc. Natl. Acad. Sci.*, vol. 100, no. 20, pp. 11547–11552, Sep. 2003.

[68]   Z. Chen, J. Guo, K. Zhang, and Y. Guo, "TP53 Mutations and Survival in Osteosarcoma Patients: A Meta-Analysis of Published Data," *Dis. Markers*, vol. 2016, pp. 1–5, 2016.

[69]   H. Köksal, E. Müller, E. M. Inderberg, Ø. Bruland, and S. Wälchli, "Treating Osteosarcoma with <scp>CAR</scp> T cells," *Scand. J. Immunol.*, vol. 89, no. 3, p. e12741, Dec. 2018.

[70]   N. Ahmed *et al.*, "Human Epidermal Growth Factor Receptor 2 (HER2) –Specific Chimeric Antigen Receptor– Modified T Cells for the Immunotherapy of HER2-Positive Sarcoma," *J. Clin. Oncol.*, vol. 33, no. 15, pp. 1688–1696, May 2015.

[71]   R. A. Morgan, J. C. Yang, M. Kitano, M. E. Dudley, C. M. Laurencot, and S. A. Rosenberg, "Case Report of a Serious Adverse Event Following the Administration of T Cells Transduced With a Chimeric Antigen Receptor Recognizing ERBB2," *Mol. Ther.*, vol. 18, no. 4, pp. 843–851, Apr. 2010.

[72]   M. Uhlen *et al.*, "Tissue-based map of the human proteome," *Science (80-.).*, vol. 347, no. 6220, pp. 1260419–1260419, Jan. 2015.

[73]   N. L. Bray, H. Pimentel, P. Melsted, and L. Pachter, "Near-optimal probabilistic RNA-seq quantification.," *Nat. Biotechnol.*, vol. 34, no. 5, pp. 525–7, 2016.

[74]   Y. Benjamini and Y. Hochberg, "Controlling the False Discovery Rate: A Practical and Powerful Approach to Multiple Testing," *J. R. Stat. Soc. Ser. B*, vol. 57, no. 1, pp. 289–300, Jan. 1995.

[75]   J. R. Moll, "Designed heterodimerizing leucine zippers with a ranger of pIs and stabilities up to 10-15 M," *Protein Sci.*, vol. 10, no. 3, pp. 649–655, Mar. 2001.

[76]   C. Zheng *et al.*, "Clinicopathological and prognostic significance of PD-L1 expression in sarcoma," *Medicine (Baltimore).*, vol. 97, no. 25, p. e11004, Jun. 2018.

[77]   W. LIANG, B. GAO, G. XU, D. WENG, M. XIE, and Y. QIAN, "Possible contribution of aminopeptidase N (APN/CD13) to migration and invasion of human osteosarcoma cell lines," *Int. J. Oncol.*, vol. 45, no. 6, pp. 2475–2485, Dec. 2014.

[78]   V. A. Siclari and L. Qin, "Targeting the osteosarcoma cancer stem cell," *J. Orthop. Surg. Res.*, vol. 5, no. 1, p. 78, 2010.

[79]   J. A. Tom *et al.*, "Identifying and mitigating batch effects in whole genome sequencing data," *BMC Bioinformatics*, vol. 18, no. 1, pp. 1–12, 2017.

[80]   J. Ahn *et al.*, "Comparative expression profiling of testis-enriched genes regulated during the development of spermatogonial cells," *PLoS One*, vol. 12, no. 4, p. e0175787, Apr. 2017.

[81]   J. Feldwisch *et al.*, "Design of an Optimized Scaffold for Affibody Molecules," *J. Mol. Biol.*, vol. 398, no. 2, pp. 232–247, 2010.

[82]   M. W. Traxlmayr *et al.*, "Strong Enrichment of Aromatic Residues in Binding Sites from a Charge-neutralized Hyperthermostable Sso7d Scaffold Library," *J. Biol. Chem.*, vol. 291, no. 43, pp. 22496–22508, Oct. 2016.

[83]   J. H. Park, M. B. Geyer, and R. J. Brentjens, "CD19-targeted CAR T-cell therapeutics for hematologic malignancies: interpreting clinical outcomes to date," *Blood*, vol. 127, no. 26, pp. 3312–3320, Jun. 2016.

[84]   R. Weinkove, P. George, N. Dasyam, and A. D. McLellan, "Selecting costimulatory domains for chimeric antigen receptors: functional and clinical considerations," *Clin. Transl. Immunol.*, vol. 8, no. 5, p. e1049, Jan. 2019.

[85]   M. Sanchez-Lockhart *et al.*, "T Cell Receptor Signaling Can Directly Enhance the Avidity of CD28 Ligand Binding," *PLoS One*, vol. 9, no. 2, p. e89263, Feb. 2014.

[86]   K. Okkenhaug and R. Rottapel, "Grb2 Forms an Inducible Protein Complex with CD28 through a Src Homology 3 Domain-Proline Interaction," *J. Biol. Chem.*, vol. 273, no. 33, pp. 21194–21202, Aug. 1998.

[87]   S. Maignan, J. Guilloteau, N. Fromage, B. Arnoux, J. Becquart, and A. Ducruix, "Crystal structure of the mammalian Grb2 adaptor," *Science (80-.).*, vol. 268, no. 5208, pp. 291–293, Apr. 1995.

[88]   R. M. Young *et al.*, "Enhancing CAR T cell persistence through ICOS and 4-1BB costimulation," *JCI Insight*, vol. 3, no. 1, pp. 1–17, 2018.

[89]   C. Quintarelli *et al.*, "Choice of costimulatory domains and of cytokines determines CAR T-cell activity in neuroblastoma," *Oncoimmunology*, vol. 7, no. 6, pp. 1–16, 2018.

[90]   A. J. Mutsaers and C. R. Walkley, "Cells of origin in osteosarcoma: mesenchymal stem cells or osteoblast committed cells?," *Bone*, vol. 62, pp. 56–63, 2014.

[91]   M. Ishikawa and Y. Yamada, "The Role of Pannexin 3 in Bone Biology," *J. Dent. Res.*, vol. 96, no. 4, pp. 372–379, 2017.

[92]   S. R. Bond *et al.*, "Pannexin 3 is a novel target for Runx2, expressed by osteoblasts and mature growth plate chondrocytes," *J. Bone Miner. Res.*, vol. 26, no. 12, pp. 2911–2922, 2011.

[93]   N. Hanagata, "IFITM5 mutations and osteogenesis imperfecta," *J. Bone Miner. Metab.*, vol. 34, no. 2, pp. 123–131, 2016.

[94]   H. Hojo, S. Ohba, X. He, L. P. Lai, and A. P. McMahon, "Sp7/Osterix Is Restricted to Bone-Forming Vertebrates where It Acts as a Dlx Co-factor in Osteoblast Specification," *Dev. Cell*, vol. 37, no. 3, pp. 238–253, May 2016.

[95]   B. Hou, Y. Tang, W. Li, Q. Zeng, and D. Chang, "Efficiency of CAR-T Therapy for Treatment of Solid Tumor in Clinical Trials: A Meta-Analysis," *Dis. Markers*, vol. 2019, 2019.

[96]   I. Bozic and M. A. Nowak, "Resisting Resistance," *Annu. Rev. Cancer Biol.*, vol. 1, no. 1, pp. 203–221, 2016.

[97]   N. N. Shah, T. Maatman, P. Hari, and B. Johnson, "Multi Targeted CAR-T Cell Therapies for B-Cell Malignancies," *Front. Oncol.*, vol. 9, Mar. 2019.

[98]   H. Jia *et al.*, "Haploidentical CD19/CD22 bispecific CAR-T cells induced MRD-negative remission in a patient with relapsed and refractory adult B-ALL after haploidentical hematopoietic stem cell transplantation," *J. Hematol. Oncol.*, vol. 12, no. 1, p. 57, Dec. 2019.

7. Supplementary Data

Run	k_a (1/Ms)	k_{off} (1/s)	K_D (M)	R_{max} (RU)	R_{max} (theoretical)	Mean K_D
WT_21_1	1,28E+06	0,02978	2,32E-08	127,7	142	2,29E-08
WT_21_2	1,32E+06	3,00E-02	2,27E-08	127,6	142	
WT_43_1	1,31E+06	0,0298	2,28E-08	142,7	160	23 nM +/- 0,23 nM
WT_43_2	1,28E+06	0,02943	2,30E-08	144,1	160	
R10A_21_1	5,85E+05	0,3854	6,58E-07	125,3	142	6,39E-07
R10A_21_2	6,00E+05	0,3847	6,42E-07	125,4	142	
R10A_43_1	5,80E+05	0,3632	6,26E-07	141,2	160	639 nM +/- 14,5
R10A_43_2	5,75E+05	0,3622	6,30E-07	142,1	160	
R32A_21_1	8,31E+05	0,2449	2,95E-07	120,6	142	2,85E-07
R32A_21_2	8,42E+05	0,2486	2,95E-07	121,9	142	
R32A_43_1	8,60E+05	0,2403	2,79E-07	119,5	139	285 nM +/-12 nM
R32A_43_2	8,80E+05	0,2381	2,71E-07	115,9	139	

Supplementary Table 1: Raw data from all SPR runs including k_{on} values, k_{off} values, KD values as well as R_{max} and theoretical R_{max} values.

Tissue	Gewebe	Samples	Source
OS	Osteosarkom	40	INFORM registry
adrenal gland	Nebenniere	3	human protein atlas
appendix	Wurmfortsatz	3	human protein atlas
bone marrow	Knochenmark	4	human protein atlas
brain	Gehirn	3	human protein atlas
colon	Grimmdarm	7	human protein atlas
duodenum	Zwölffingerdarm	2	human protein atlas
endometrium	Gebärmutterschleimhaut	5	human protein atlas
esophagus	Speiseröhre	3	human protein atlas
fallopian tube	Eileiter	5	human protein atlas
fat	Fettgewebe	5	human protein atlas
gallbladder	Gallenblase	3	human protein atlas
heart	Herz	4	human protein atlas
kidney	Nieren	4	human protein atlas
liver	Leber	3	human protein atlas
lung	Lunge	5	human protein atlas
lymph node	Lymphknoten	5	human protein atlas
mesenchymal stem cells	mesenchymale Stammzellen	2	https://doi.org/10.1073/pnas.1716164115
osteoblasts	Osteoblasten	4	10.1007/s00198-013-2529-9
ovary	Eierstock	3	human protein atlas
pancreas	Pankreas	2	human protein atlas
placenta	Plazenta	3	human protein atlas

prostate	Prostata	4	human protein atlas
rectum	Rektum	4	human protein atlas
salivary gland	Speicheldrüse	3	human protein atlas
skeletal muscle	Skelettmuskulatur	5	human protein atlas
skin	Haut	3	human protein atlas
small intestine	Dünndarm	3	human protein atlas
smooth muscle	glatte Muskulatur	3	human protein atlas
spleen	Milz	4	human protein atlas
stomach	Magen	3	human protein atlas
testis	Hoden	7	human protein atlas
thyroid gland	Schilddrüse	4	human protein atlas
tonsils	Mandels	3	human protein atlas
urinary bladder	Blase	2	human protein atlas

Supplementary Table 2: List of all tissues included in bioinformatic analysis